Modeling the effects of sand mining in river-dominant delta-systems

Master Thesis Environmental Engineering

ENVM4010

Camu Prins

Delft University of Technology

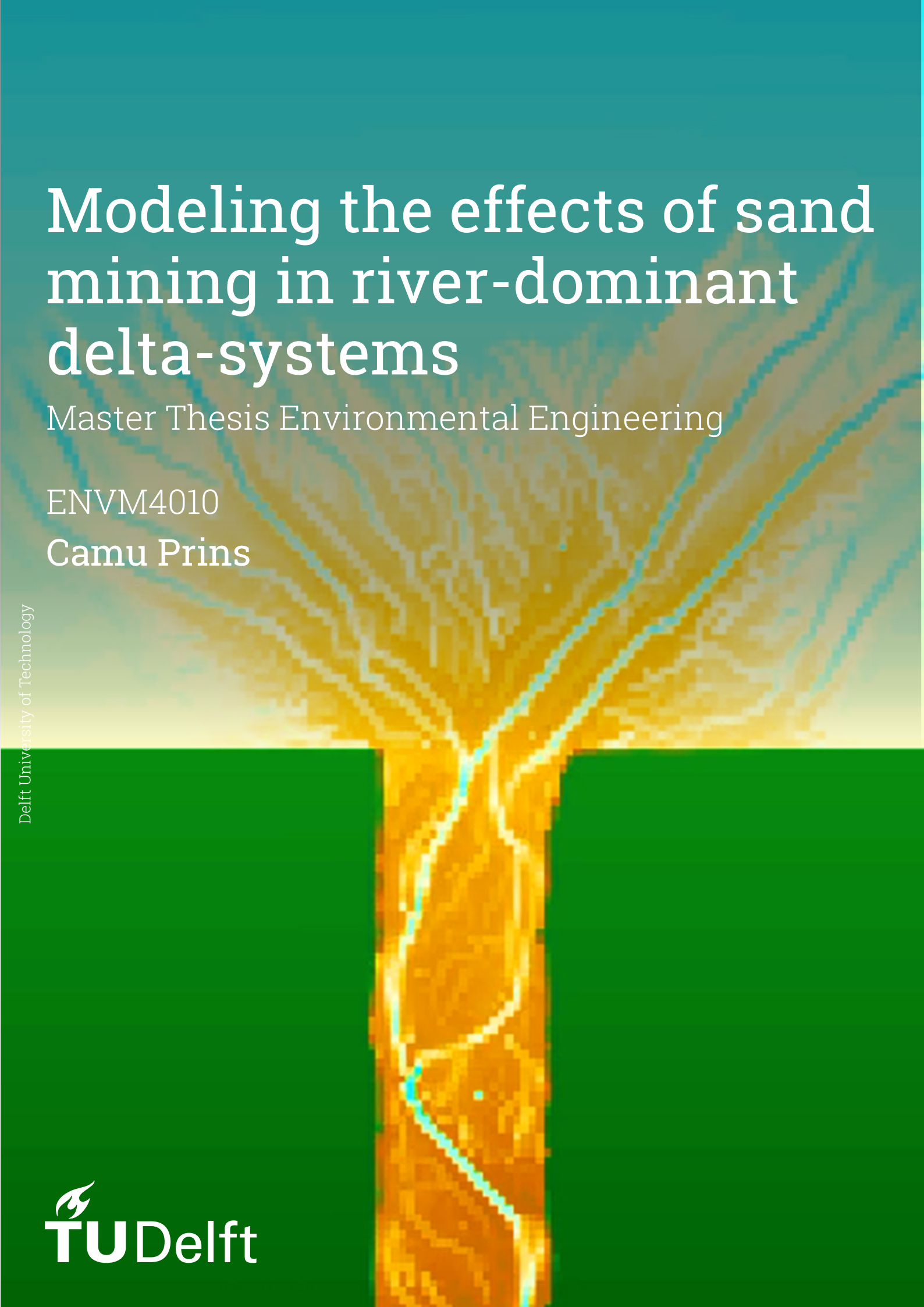

TU Delft

Modeling the effects of sand mining in river-dominant delta-systems

Master Thesis Environmental Engineering

by

Camu Prins

to obtain the degree of Master of Science

at the Delft University of Technology,

to be defended publicly on Wednesday July 16, 2025 at 15:00.

Student number:	5655838
Thesis duration:	March, 2025 – July 16, 2025
Thesis committee:	Dr. A. Baar, TU Delft, supervisor
	Dr S. Toby, TU Delft

Cover: The DELFT3D model of a river and delta system used in this thesis.

TU Delft

Abstract

Sand mining is a growing environmental and socioeconomic concern worldwide. As urbanisation and infrastructure development continue to increase, the demand for sand has skyrocketed. When mined on or near rivers, it alters the river's pathway, eroding riverbanks, damaging housing, infrastructure and livelihoods. This thesis examines the role of sand mining in the river-delta system, by examining the influence of dredging duration, dredging intensity, location and pit size on the river delta system.

A 2-dimensional depth averaged Delft3D model is made. Here a river-delta system is modelled and run for 600 years. Over the last 100 years, different sand mining scenarios have been modelled. With varying duration, intensity, locations, and pit geometry, each of these scenarios is then analysed using various method of analyses. Though changing the dredging scenarios, changes the downstream morphology and hypothe- sised trends—such as pit migration, increased erosion, and reduced delta growth—were partially observed. Furthermore, in the five scenarios, dredging influenced the river-delta system in complex, non-linear ways.

Some configurations (e.g., 30-year duration, 5.0x intensity, 200 m width) led to pronounced short-term changes, but long-term outcomes returned toward control-like conditions. In general, the results highlight high internal variability and limited predictability based solely on single dredging parameters. It is recommended to include a cluster of slightly varied control scenarios in future research to distinguish the effect of dredging from the natural variability of the river.

Contents

List of Figures

List of Tables

1

Introduction

1.1. Global Context and Impacts of Sand Mining

Sand mining is a growing environmental and socio-economic concern worldwide. As urbanization and infrastructure development continue to surge, the demand for sand - a vital component in construction - has skyrocketed. Sand can be mined in multiple ways, either through an open pit (sand pit), by mining of beaches and inland dunes, or through dredging of shorelines and river beds (Hernandez et al., 2021). In contrast to desert and ocean sand, which is too soft for construction, sand deposits in riverine and coastal environments often exhibit the ideal grain size and shape for construction. Making it a valuable resource and a target for exploitation world wide. Filho et al. (2021) provides an overview of countries affected by this issue. In South Asia, countries like India, Nepal, and Sri Lanka face extensive, often illegal, river sand extraction, leading to riverbank collapse, groundwater depletion, and habitat loss. For example, Nepal's Kathmandu Valley extracts over 3,000 m^3 daily, with nearly half unregulated. In Africa, South Africa and Ghana report river and coastal mining, causing erosion and salinization. China and Vietnam continue large-scale dredging on rivers like the Yangtze and Mekong, despite environmental damage. In America, the U.S. and Brazil have long histories of coastal and river mining, key sites include California's Monterey Bay and Brazil's Paraíba do Sul River. Also, in Europe, sand mining in the rivers is taking place, for example in Croatia (WWF, 2020). Though environmental activist where able to stop this activity. These cases reflect a global trend of poorly regulated sand extraction with severe ecological impacts. Countries not mining rivers or coasts rely on land pits or imports. In 2023, the top sand importers were the United States, the Netherlands, Australia, Germany, and Cambodia, with global sand trade worth $2.4 billion (HarvardGrwthLab, 2023).

The method of extraction depends on where the desired sand is located. Along rivers, sand is dug up, using big machinery, shovels, or bare hands. Along coastlines and on the river, miners utilize dredging boats or suction pumps (Da & Billon, 2022). These boats disrupt the natural system and leave big gaps in the river bed. These gaps result in a changing river course and cause river banks to erode (Hackney et al., 2020). Furthermore, by removing sand upstream, the total amount of sediments that naturally replenishes sediment stored in river beds is reduced. This reduced sediment causes downstream bed alterations (Hackney et al., 2020; Kim et al., 2023; Nguyen et al., 2024), due to a lowered bed level. When the bed height is lowered sufficiently, river banks are eroded, potentially damaging housing, and infrastructure and threatening livelihoods (Lawal, 2011; Padmalal et al., 2007; Wang et al., 2012). Also, mining on river banks causes rivers to further expand, as the mining equipment to dig up sand along the river bank needs space, and vegetation is removed. This destabilizes the bank and causes further erosion, as vegetation stabilises river banks (Arora & Kumar, 2024).

Next to morphological changes, the harmful effect of sand mining on aquatic ecosystems has been studied. Reducing biodiversity by removing vital components of a marine ecosystem, such as invertebrates, microorganisms and meiofauna (Koehnken & Rintoul, 2018). The turbidity caused by mining further decreases the water quality, by reducing the amount of light that micro-organisms and small water creatures depend on. This is linked to the loss of shellfish fish populations and is linked to the destruction of spawning habitats (Koehnken et al., 2020).

Besides these environmental effects, the social impacts of sand mining are an extensive list. Working in this industry is often under-paid, done by children and is an insecure source of income (Bendixen et al., 2019; Schandl et al., 2017). As Rentier and Cammeraat (2022) – whom made an extensive overview of the impacts – put it: The sand mining industry creates jobs, but the circumstances under which people word and the effects on the environment and livelihood, are detrimental. Furthermore, the loss of beach areas contributes to a reduced tourism industry, which is also affected by damage to coastal infrastructure (Shaghude et al., 2012). On top of that, food security and agriculture are affected (Padmalal & Maya, 2014). With a broader river and deeper channels, come an increased saline intrusion in deltas and freshwater sources. With a degrading ecosystem and habitat destruction, also comes a reduced possibility for fishing (Da & Billon, 2022).

While a lot of sand mining is regulated, the increased demand has given rise to unregulated criminal mining operations that exploit riverbeds, beaches and local communities. As these practices not only deplete natural resources at unsustainable rates but also disrupt aquatic ecosystems and cause erosion, it is important to realize the scale at which this happens. In India, the scale of crime related to sand mining has gotten so big, that it is referred to as the 'Sand Maffia' (Mouterde & Depardon, 2023). The article also highlights the stories of miners who are forced to work in this industry, explaining that they have no other option to feed their families and that they work in fear of getting caught by the police. And this is only one of the locations at the Son River.

1.2. Morphological Effects of Sand Mining

A river flows continuously and achieves a regime condition with no overall deposition or erosion at larger spatial and temporal scales, unless an intense or large-scale natural event or anthropogenic activity disrupts the river balance. Locally, however there is constant dynamic activity. The river continuously erodes, transports, and deposits sediment, but these small-scale processes tend to balance out over time and space. Once disrupted, the river adjusts to a new equilibrium by depositing incoming sediment near the disturbance site, eroding the surrounding areas, or altering its flow path to accommodate changes (Thorne & Tovey, 1981).

On a local scale, the sand pits cause a chain of physical and hydrological changes. When sand is removed, the river begins to erode their own beds and banks to compensate for the missing sediment. The upstream edge of a pit is called the nickpoint (Hackney et al., 2020). Here the water drops into the pit, causing erosion. The pit migrates upstream, also called head cutting (Kondolf, 1997). At the same time, as sand pits are being replenished, the river becomes sediment hungry. This enhance the capacity of the river to erode the channel more aggressively downstream (Arora & Kumar, 2025; Kondolf, 1997; Padmalal & Maya, 2014).

In terms of cross-sectional changes, pit excavation cause the channel to become deeper and wider. This widening is caused by incision and bank failure, especially when riverbanks are undercut by mining (Bhattacharya et al., 2019; De Leeuw et al., 2009; Erskine, 2008). As the nick point migrates upstream, its incision and bank undercutting release additional sediment

to downstream reaches where the channel may aggregate and become unstable. For example, the mainstem Russian River in California. Its nickpoint propagated up to its tributary Dry Creek, where undercutting of banks, channel widening (from 10 to 400 meters in places), and destabilisation, increasing delivery of sand and gravel to the mainstem Russian River(Kondolf, 1997). In the case where sand is mined close to the active channel, the instability can cause pit walls to collapse and merge with the river, also known as pit capture.

Sand mining causes significant changes in the movement of both suspended and bedload sediment further downstream. The sediment-deficient, or "hungry," water increases the flow's capacity to erode riverbeds below mining sites. Although this phenomenon is recognised, the extent and scale of its downstream impacts remain understudied (Arora & Kumar, 2025). Similarly, dams also generate hungry water conditions, destabilising downstream reaches and reducing sediment delivery to many coastal areas. These effects have been studied and are known to contribute to accelerated beach erosion, dune erosion, and coastal land loss (Kondolf, 1997; Shaghude et al., 2012; Stanley, 1996). The flow pattern changes caused by sand mining needs further research, as shifting sediment regimes can drastically reshape riverine and coastal environments, and their long-term effects are still not fully understood. These coastal regions are critically important for the safety and livelihood of the people living in them. Over 500 million people are estimated to live on deltas, with even more living along major rivers (Edmonds et al., 2020). For infrastructure planning and housing, it's essential to better understand the downstream impacts of these disturbances, and whether the negative effects of mining practices can be reduced.

As global demand for sand continues to rise, these challenges are unlikely to disappear. We still know little about how sand mining affects delta formation and downstream erosion. Mapping out and modelling the outcomes of different mining techniques, as this could help establish a more sustainable balance between the natural supply of sediment and extraction rates.

Some key river systems experiencing intense sand mining include the Godavari, Volga, Niger, and Mekong. These river-dominated systems depend heavily on continuous sediment supply to maintain morphological equilibrium. Human interventions like mining interrupt this balance, often resulting in channel incision, delta retreat, and increased flood risk.

1.3. Modelling Sediment Transport and Morphology

Effects of sand mining can be modelled through laboratory experiments (Arora & Kumar, 2025; Barman et al., 2018; Bhattacharya et al., 2019; Haghnazar et al., 2020) and through numerical modelling (Kim et al., 2023; Maaß & Schüttrumpf, 2018; Nguyen et al., 2024) to simulate the sediment transport and the morphological change. These models have proven effective in explaining both localized and system-wide effects. For example, Thi Kim et al. (2020) modelled sections of the Mekong Delta under both natural and mining-influenced conditions and successfully explained observed channel erosion patterns with modelled sand extraction scenarios. Similarly, Maaß and Schüttrumpf (2018) demonstrated that mining-induced subsidence reduced the sediment trapping efficiency of floodplains, leading to further morphological degradation.

In another study, Haghnazar et al. (2020) investigated the pit infilling process, the gradual refilling of mined areas by sediment. By varying pit geometries and spacing, they found optimal configurations that minimize negative impacts and maximize efficiency at the local scale. Specifically, they identified that when the pit length-to-width ratio (l/b) was 0.78 and 0.59, the optimal pit spacing relative to stream depth (L/y) was 20 and 16, respectively. While useful for planning and economic efficiency, these optimizations primarily focus on localized impacts and

often overlook how such interventions influence morphological changes further downstream.

While the literature provides a strong foundation for understanding the local impacts of sand mining, relatively few studies have addressed the downstream morphological response at larger spatial scales. In particular, the influence of sand mining practices on the riverbed and delta morphology kilometres downstream remains underexplored. This is a critical knowledge gap, especially in sediment-starved systems where downstream impacts may be delayed or distributed over long distances.

1.4. Research Objectives and Approach

In this thesis, a hydro-morphodynamic numerical model will be used to simulate a river-dominated estuarine system under different sand mining scenarios. The model will be used to explore how various parameters—such as pit location, pit shape, volume of extraction, and duration of extraction—influence the downstream morphology. The modelling domain is designed to capture changes downstream of the mining area, allowing for analysis of morphological consequences. A control scenario without mining will be included to isolate the effect of sand extraction.

This modelling approach will allow for a systematic investigation of sediment redistribution and channel evolution under different mining strategies, thereby offering insights that are relevant for sustainable river and delta management.

The central research question guiding this thesis is:

How does the downstream morphology of a river-dominated delta change under the influence of sand mining practices?

In this context, "downstream morphology" refers to the evolution of bed level changes and sediment patterns occurring from the last mining site to the river mouth of the Delta. This includes both the river channel and the deltaic region. The degree of morphological change will be assessed by comparing mining scenarios to the control scenario with no sand extraction.

To comprehensively address the main research question, the following sub-questions are formulated:

1. What is the influence of the volume of sediment extraction on the downstream morphology of a river-dominated delta?
2. What is the influence of dredging duration on the downstream morphology of a river-dominated delta?
3. What is the influence of extracting sediment at a single location versus multiple separate locations on the downstream morphology of a river-dominated delta?
4. What is the influence of pit length on the downstream morphology of a river-dominated delta?
5. What is the influence of pit width on the downstream morphology of a river-dominated delta?

The insights gained through this study aim to contribute to the broader understanding of sediment dynamics in river-dominated deltas and to inform more sustainable sand mining practices.

2

Methodology

2.1. Background of Delft3D

This study uses the process-based morphodynamic model Delft3D, which solves the depth-averaged shallow water equations along with sediment transport and bed level changes. Though a 3D-model can be made, here a two dimensional (depth averaged) model is used for efficiency. Delft3D has been applied several times for modelling rivers, estuaries, and coastal systems and is known for producing reliable results (Jenkins et al., 2024; Rahdarian & Winter, 2025; Roelvink et al., 2006; Schuurman et al., 2013). It has been validated against many well-documented flume and field cases, such as the Rhine River (Mosselman, 2004). A comparison of morphodynamic models by Langendoen (2001) showed that Delft3D, has one of the strongest theoretical foundations for sediment transport and morphological modelling.

Delft3D-FLOW solves the depth-averaged shallow water equations to simulate free-surface hydrodynamics in coastal and riverine systems. The core system includes the continuity equation for mass conservation and the horizontal momentum equations in the x and y directions. These account for pressure gradients, Coriolis effects, bed shear stress, and other forcing terms like wind stress and turbulence (Deltares, 2025).

2.2. The Experimental Setup

To set up the delta, a grid of 200 × 200 cells with a pixel size of 50 × 50 meters is used, resulting in a total research area of 10 × 10 km. The river section has a longitudinal drop of 5 meters over 10,000 meters (slope: 0.0005 [m/m]). The banks start at an elevation of 5 meters and gradually slope down to 4 meters at the coastline. A pre-dug riverbed is included to accelerate the model's convergence toward equilibrium, as it reduces the time required for the river to erode its path through the terrain. This setup allows the system to reach a steady-state condition more efficiently than if the river had to incise the entire channel from an initially flat or uniformly elevated surface.

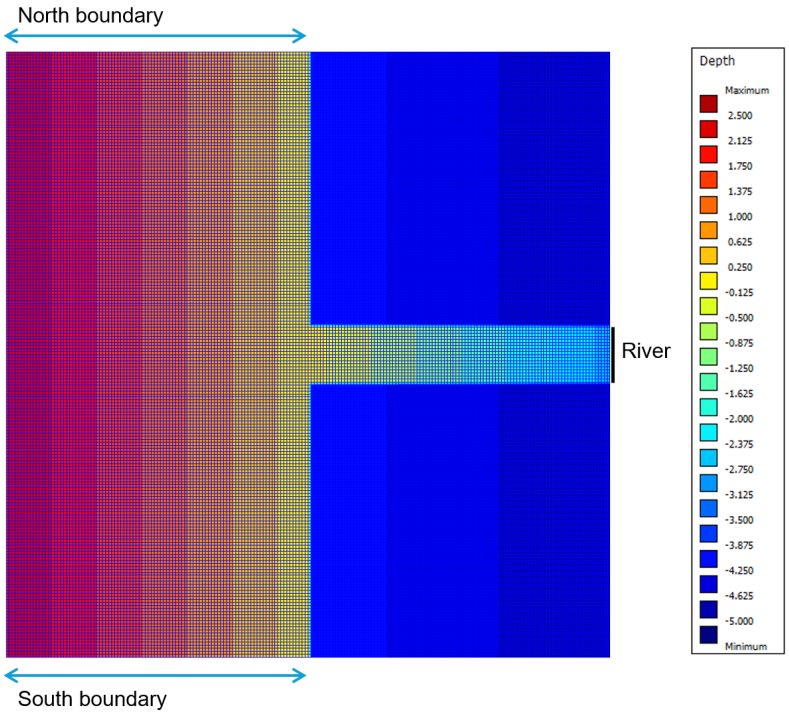

Figure 2.1: Initial bathymetry, with a slope of 0.0005 for the river and the basin, and an initial bank of 2.5 meters above the river. With a discharge boundary as the river and two harmonic water levels at the North and South boundary.

Three boundary conditions are added to the grid. On the right, there is an inflow boundary with a time series specifying a discharge of 200 m³/s under equilibrium sediment conditions. At the top and bottom of the basin, the north and south boundaries are defined, respectively. An harmonic water level is maintained. Tides are included through this harmonic condition: the water level has a harmonic forcing type, with a frequency of 30 deg/h and an amplitude of 0.5 meters at these boundaries. There is no boundary defined on the left side of the basin.

The rest of the model settings for the setup are summarised in Table 2.1.

Parameter	**Value**	**Unit**
Initial Slope	0.0005	m/m
Simulation Time (hydro / morph)	548 / 600.5479	d / y
MorFac	400	[-]
Secondary Flow	ON	-
D_{50}	200	µm
Specific Density	2650	kg/m³
Dry Bed Density	1600	kg/m³
Factor for Erosion Adjacent Dry Cells	0.5	-
Spin-up Interval	720	min
Time step	0.5	min
Minimum Depth for Sediment Calculation	0.1	m
Sediment Transport Predictor	Engelund–Hanssen	
AShield factor	0.8	-
Bshield factor	0.5	-

Table 2.1: Model parameters used for the setup

In order to simulate the sediment, two commonly used transport predictors can be applied: Van Rijn and Engelund–Hansen. Here, the Engelund–Hansen method (Engelund & Hansen, 1967) is used, as it has been shown to be more effective in sand-based environments and produces less river incision or steeper slopes than those typically observed in nature (Brownlie, 1982).

To account for transverse sediment transport, the longitudinal sediment transport is modified. Two approaches that can be used are the Ikeda (Ikeda, 1989) method and the Koch & Flokstra (Koch & Flokstra, 1981) method. The difference lies in how sediment transport is calibrated to respond to slope: Koch & Flokstra rotate the sediment transport vector derived from the predictor by a certain factor, while Ikeda multiplies the sediment predictor with a perpendicular downslope vector, thereby increasing the total sediment transport predicted. Effect of the choice is great, also illustrated by Baar et al. (2019).

In this study, the Koch & Flokstra method is chosen, based on early experimental comparisons between the two. In Appendix C, both the Koch & Flokstra method (Figure C.3) and the Ikeda method (Figure C.2) are applied. The Koch & Flokstra method is tested using the parameter A_{sh} in a range between 0.2 and 0.8. The Ikeda method is tested using values of α_{Bn} = 1.5 , 5, 10, and 30. Based on visual interpretation of these results and on the attempted to minimize creating unrealistic transverse sediment transport, this study uses the Koch & Flokstra method with the parameters $A_{\text{sh}} = 0.8$ and $B_{\text{sh}} = 0.5$.

Furthermore, in a similar manner the Morphological acceleration factor is tested in Appendix B Figure C.1. As it is attempted to look on a developed delta and to keep calculation times minimal, it is beneficial to use a large MorFac. It is used to speed up long-term bed evolution relative to the hydrodynamic time step and is set at 400, based on van der Wegen and Roelvink (2008) and the test conduted in Appendix B.

Only grid cells with water depths greater than 0.1 m are active for sediment transport. Bank erosion is handled by allowing dry cells next to eroding wet cells to also erode. When this happens, 50% of the bed level drop in the wet cell is transferred to the neighbouring dry cell.

After 600 years, the bathymetry has evolved as shown in Figure 2.2. The river appears to be in equilibrium within the boundaries provided in Figure 2.1. The shape of the delta is not perfectly circular; instead, it has developed into a distinctive V-shape. In order to ensure that the river has reached its full meander width, Year 500 was selected. By this point, the riverbanks have been fully eroded, and the channel appears to have reached a consistent width. Additionally, the delta's overall size and shape slightly resemble the Mahakam Delta, which served as the basis for the initial model inputs (see Appendix A for reference). Based on these observations, the 500-year mark is chosen as the point at which sand mining is implemented. At this stage, the delta is well-developed and exhibits a stable and balanced morphology, making it an appropriate moment for dredging interventions.

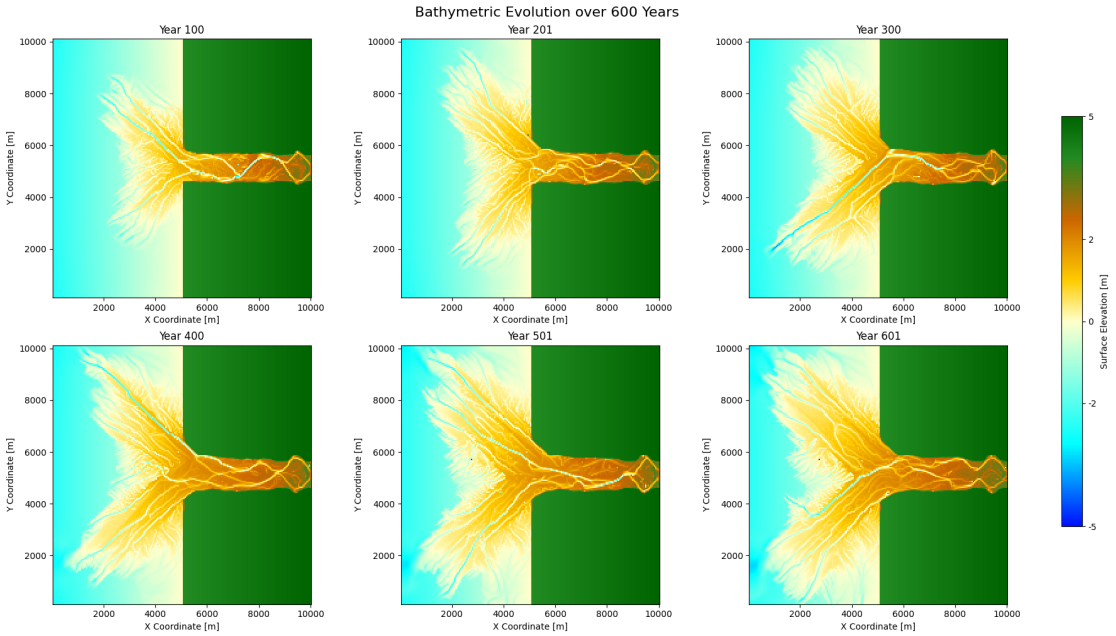

Figure 2.2: Bathymetry Evolution of 600 years.

In order to relate the dredged sediment volumes to real-world scenarios, the ratio between the dredged volume and the sediment concentration of the river is used as a basis for different scenarios. Throughout most of the experiment this ratio will be one, where the sediment concentration through boundary is equal to the sediment volume leaving through dredging. When the ratio is ten, ten times the amount of sediment entering the system is being dredged. Using this ratio, it becomes possible to relate dredging volumes to real world scenarios.

The sediment concentration at the boundary is derived from the experimental setup simulation. For this setup, which runs for 600 morphological years, the average total sediment load passing through the rightmost cross-section near the boundary is used. The Engelund-Hansen transport formula, applied in Delft3D, calculates total sediment transport, combining both bedload and suspended load into a single value. Therefore, the computed load represents the total concentration, even though Delft3D may label it as ”bedload” in the output.

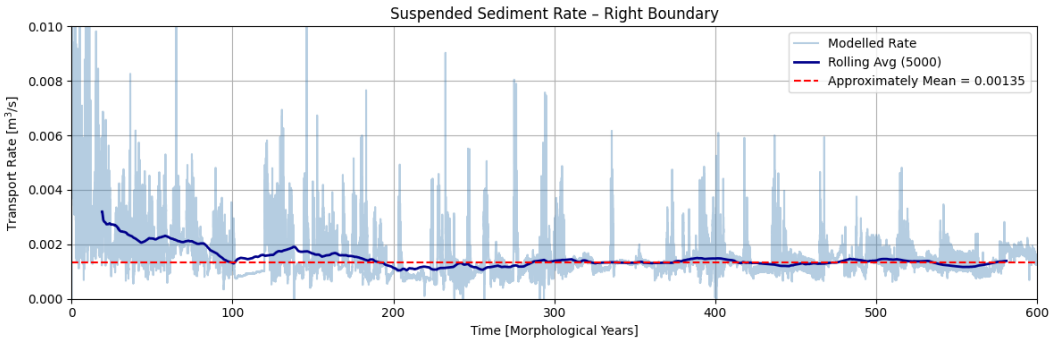

Figure 2.3: Sediment transport close to the river boundary, with a mean of 0.00135 $[\mathrm{m}^3/\mathrm{s}]$.

The bed-load transport at the cross-section is measured in cubic meters per second and stabilizes at 0.00135 m³/s (figure 2.3). This value is low, for a river of 200 m³/s, it translates to 6.75 parts per million (ppm). Suspended sediment concentrations in natural, undisturbed rivers are

typically less than 100 ppm, whereas disturbed systems can exceed 10,000 ppm during storm events or under high sediment loads(Dodds & Whiles, 2004).

This value is chosen rather than the mean over the entire simulation because the initial years were not representative, as the system still needed to stabilize. This value is converted to cubic meters per morphological year [$\mathrm{m^3/y_m}$] by multiplying it with the number of seconds in a year, dividing by the morphodynamic acceleration factor (Morfac), and adjusting for the porosity factor. This yields a rate of 176 $\mathrm{m^3/y_m}$ (44 $\mathrm{m^3/y_m}$ per pit) of sand passing through the cross-section, which corresponds to the amount removed by mining ($\mathrm{q_d}$) when the ratio of dredged material to sediment concentration at the inlet is equal.

$$q_d = \frac{q_s \cdot (3600 \cdot 24 \cdot 365)}{Morfac \cdot (1 - porosity)}$$

This base rate is used in most scenarios but is adjusted in the scenario where dredging intensity is varied. For that scenario, the extraction rates listed in Table 2.2 are used for the dredging simulations.

Rate	**0.5x**	**1x**	**2x**	**5x**	**10x**
Total [$\mathbf{m^3/y_m}$]	88	176	352	880	1760
Per pit [$\mathbf{m^3/y_m}$]	22	44	88	220	440

Table 2.2: Extraction rates under different rate scenarios

2.3. Experimental Scenarios

In the experimental setup, five different scenarios are investigated to understand the impacts of various dredging strategies on delta development. Each scenario modifies a different parameter while keeping others constant to isolate its effect.

Scenario	**Variable Parameter**	**Test Values**
Scenario 1: Varying Dredging Duration	Duration of mining (years)	10, 20, 30, 40, 50
Scenario 2: Varying Dredging Intensities	Sand extraction rate	0.5×, 1.0×, 2.0×, 5.0×, 10.0×
Scenario 3: Varying Dredging Groups	Number of dredging locations	4 pits, 2 pits, 1 pit
Scenario 4: Varying Pit Length	Length of each pit	50, 100, 150, 200 m
Scenario 5: Varying Pit Width	Width of each pit	50, 100, 150, 200 m

Table 2.3: Overview of Experimental Scenarios

For the majority of scenarios, the sand mining pits and extraction rates are held constant. The pits are located in the upstream section of the river, with the final pit positioned 2,500 meters from the delta. Each pit measures 50 by 50 meters and is spaced 500 meters apart (Figure 2.4). Sand is extracted at a rate of 44$\mathrm{m^3/y_m}$ per pit, resulting in a total of 176 $\mathrm{m^3/y_m}$ across all pits—equal to the incoming sediment load from the river boundary. This ensures a balanced sediment budget: what enters the system is removed through dredging.

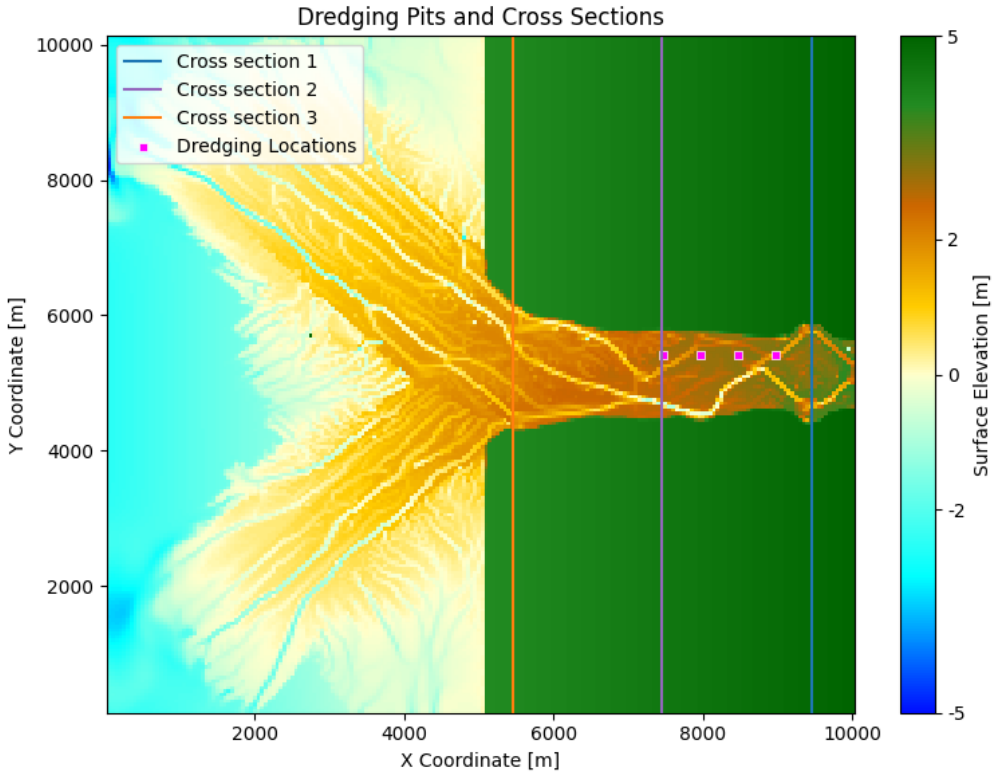

Figure 2.4: Model domain with the locations of the mining pits and the cross sections.

To examine the effects of mining duration on delta development, simulations are conducted with time steps of 10, 20, 30, 40, and 50 years. The sediment extraction rate remains constant, using the same pit configuration as described above, this concludes the first scenario.

In the second scenario, the amount of sand mined is varied, while the duration is kept constant at 10 morphological years. The sand extraction rates correspond to half the sediment input (0.5x), equal to the sediment input (1.0x), twice, five times, and ten times the sediment input. The corresponding dredging volumes are calculated and presented in Table 2.2.

To investigate the effect of pit grouping, configurations with four, two, and one mining location are tested. All configurations are mined for 10 years, and the total sediment extracted is kept constant at 176 $\mathrm{m}^3/\mathrm{y_m}$. The total area of the pits is also consistent across all cases, with a combined area of 200 × 200 meters.

To investigate the effect of pit length, the same locations as shown in Figure 2.4 are used. The duration is set to 10 years, and the total dredged volume remains constant at 176 $\mathrm{m}^3/\mathrm{y_m}$. The impact of pit length is tested by elongating the pits in four steps: 50, 100, 150, and 200 meters in length. As the pits become longer, the distance between them decreases accordingly.

Similar to the variation in length, the effect of pit width is examined using the same method. The locations illustrated in Figure 2.4, a duration of 10 years, and a total volume of 176$\mathrm{m}^3/\mathrm{y_m}$ are used. The impact of width is tested by widening the pits in four steps: 50, 100, 150, and 200 meters. In this scenario, the distance between the pits is kept constant.

2.4. Methods of Analysis

The Method of analyses consists of five parts: Visual analysis, Braiding Index, Size of the Delta, Sand Balance and Rate of Change.

The visual analysis provides an initial assessment of morphological changes the downstream area by comparing each experimental scenario to the control simulation, in which no sand mining occurs. In addition, the 10-year, 1.0x extraction scenario is used as a reference case for interpreting the relative effects of varying parameters. Key indicators include whether stream alteration has occurred, changes in delta shape, shifts in the spatial distribution of sand banks, and signs of landward transgression or bank erosion. Differences in the rate at which these changes develop are also considered. This qualitative assessment offers essential context for interpreting the quantitative results that follow.

There are a number of ways to indicate the braiding intensity of a river, for example by measuring the total length of channels or bars per reach (Sinuosity Index, bar Index), or by counting the number of channels per cross-section (Egozi & Ashmore, 2008). A channel count index is preferred due to its insensitivity to variations in channel sinuosity and orientation. It has the smallest coefficients of variations and can be measured quickly and reliably in experiments. In this experiment, the method of channel counting is used. Similar to Schuurman et al. (2013), the number of parallel channels (Total Braiding Index) is counted in all cross-sections over each time step. However, rather then using the cross-sectional average bed elevation, the bottom shear stress is used as a threshold. This is done to account only for active channels, rather than including channels that have dried up. The Active Braiding Index (Bertoldi et al., 2009) includes only active channels with enough stress for erosion to occur. In this setup, the shear varies between 0 and 5 N/m^2, a constant threshold value of 0.5 N/m^2 is used to determine whether or not a section has flowing water over it and is thus functioning as a channel. The Braiding Index is also taken over the entire river at two time steps. This creates a distribution of the BI, which is tested using a Kolomogorov-Smirnov test, in order to check if the structure of the river reach is significantly different from the control scenario.

Another important aspect of this study is assessing the growth rate and overall size of the delta. At each time step, the delta size is determined using the OpenAngleMethod proposed by Shaw et al., 2008. Unlike traditional methods that rely on the land-water interface, this approach uses the visibility or ”open angle” to open water. This is advantageous because the land-water interface method can exclude the river itself from the delta outline, especially near the river mouth, whereas the Open Angle Method properly includes the river channel as part of the delta. In practice, at every time step, the viewing angle from each pixel to a predefined open water region is calculated. Pixels with viewing angle of 45 degrees are classified as ocean, while those below are considered part of the delta. Both the opening viewing angle and the blur factor are calibtrated (Figure D.1 and D.2)

A sand balance model will be developed to quantify changes in net sediment storage within the river reach and to assess whether sediment input to the delta is increasing or decreasing. This balance will help identify whether sediment is being deposited or eroded along the system, allowing for a better understanding of sediment dynamics between the inflow, sinks, and the delta.

The rate of change in elevation is calculated between each consecutive time step. For each interval, the elevation data is compared to the previous time step to identify changes. Cells where elevation decreases are classified as erosion, while cells with elevation increases are classified

as deposition. The total area of this eroded or deposited region represents the rate of change, which will be used for further analysis.

Each of these methods uses custom code to handle both the delineation and the quantitative analysis of results. More detailed explanations, particularly for the delineation process and how the Braiding Index is calculated, can be found in the GitHub repository (Prins, 2025).

3

Results

This chapter presents the results of the dredging simulations, where first a visual analysis is done on the morphology, then the results for each of the method of analysis are highlighted, and finally the different methods for each varied parameter are combined to investigate general trends.

3.1. Visual Assessment

The first thing to asses from the visual analysis to characterise the pit behaviour. The pits are visible in the figures by a slight change in pixel colour compared to the sediment around it. There are two main things visible directly around the dredging pit. The first thing is that the pit can either be dug in the river bank or directly into the channel. When it is dug in the channel, the pit is not visible in the morphology, while the pits on the bars are visible. These pits disappear again ones the river flows over the pit, showing the behaviour of pit capture.

The second thing to see around the pits is that the pit can have a permanent impact even in year 95 (Figure 3.1). In this simulation, a single dredging pit was positioned directly within the main river path from the very beginning. As a result, the pit remained in continuous contact with the river throughout the entire simulation period. This close interaction appears to have facilitated a continuous pit capture. From the earliest timesteps, the pit was actively engaged in the river's hydrodynamics, and over time, it became increasingly pronounced in both depth and shape. Visual inspection of the simulation snapshots reveals that despite minimal lateral migration, the pit evolved into a significantly deeper feature by the end of the simulation. This deepening suggests ongoing erosion or scouring processes driven by concentrated flow. Due to the scale the result, it is unclear of pit migration is occurring. Migration is a small scale effect caused by the local erosion of the nickpoint. The scouring processes could indicate pit migration.

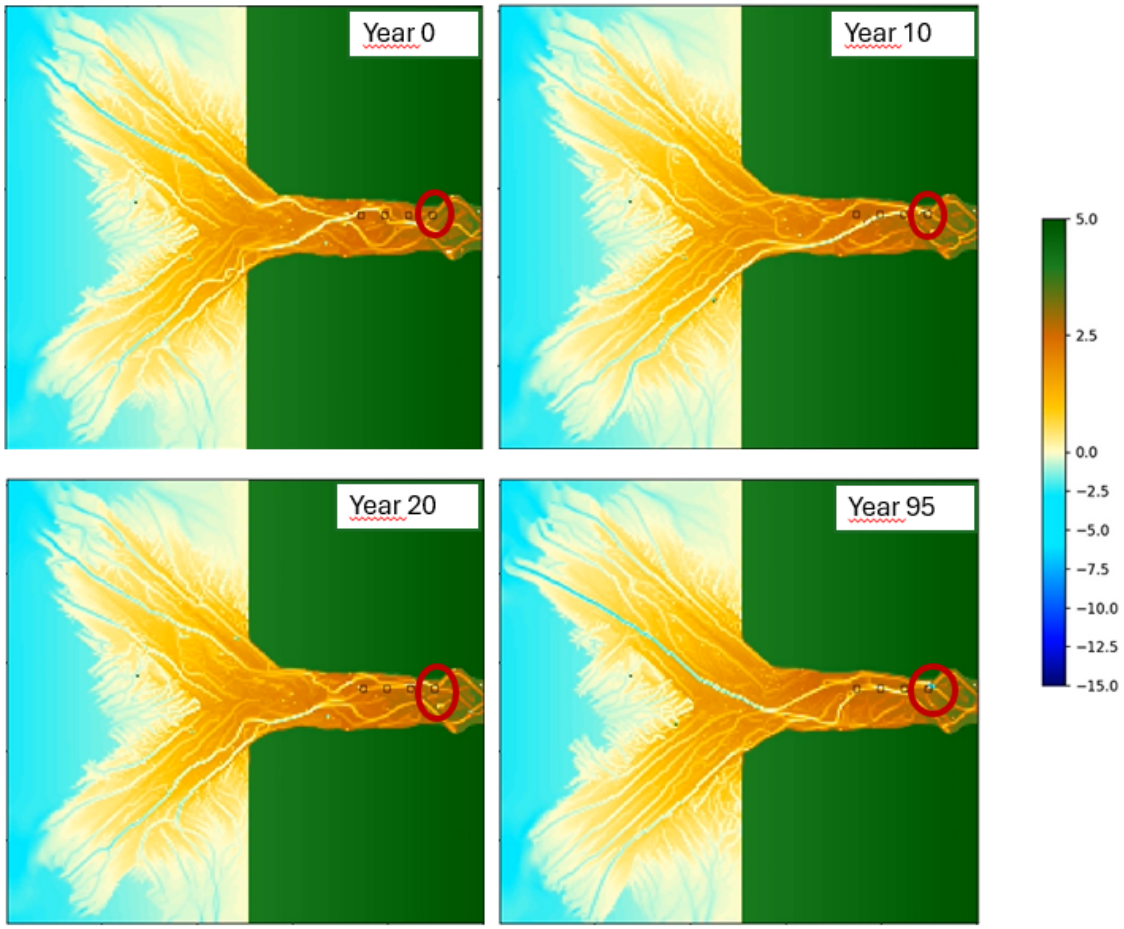

Figure 3.1: The progression of a mining pit for the grouped scenario with one mining location circled in red.

Further into the delta, other dynamics are noted, which can also be found in the growth rate analyses. First thing that is noted is that the delta is growing steadily but sometimes there are sudden accelerations of the growth. In the growth rate figure, there is a spike in the control scenario (at 50–60 years, Figure 3.6), as if something has triggered a sudden spurt of growth. This also happens in the 50-year duration scenario, the 10.0x intensity scenario, and the 100-meter pit scenario, though at different levels of intensity; for the duration scenario, it happens at a later time step.

In Figure 3.2, the moments right before and directly after are plotted. In the control scenario (3.2a), a channel near the edge of the delta got just enough shear or speed to find a different path to the sea, quickly creating a new deposition area and increasing the delta size. The 10.0x dredging intensity scenario has the same peak at the same location. This can also be seen in Figure 3.2c, where in the same location as the control scenario there is an extra deposition area. The peak for the 50-year simulation occurs differently. The location of the increased size is now in the middle rather than at the edge, though the peak is of the same magnitude as the other two situations. The sudden peak tends to occur when the river is suddenly able to find a new path. This makes sense, as in real world scenarios the same occurs when a river undergoes an avulsion, suddenly the sediment behaviour changes (Slingerland & Smith, 2004).

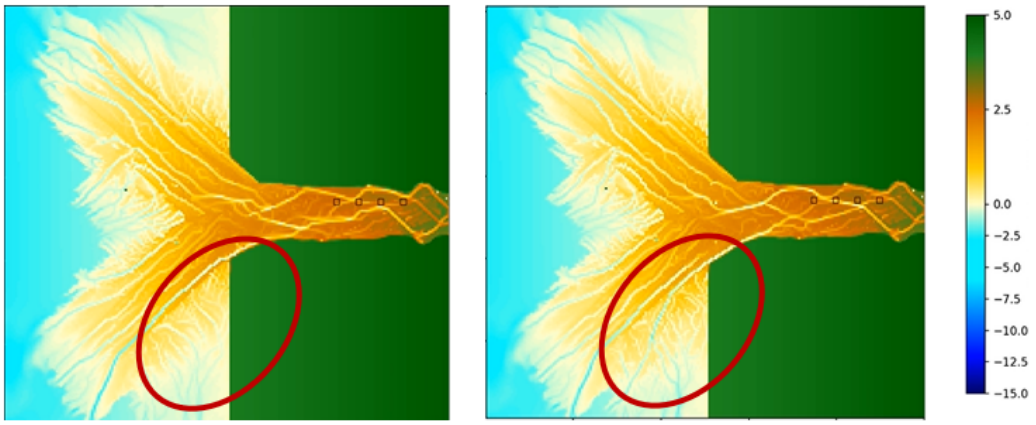

(a) Control scenario

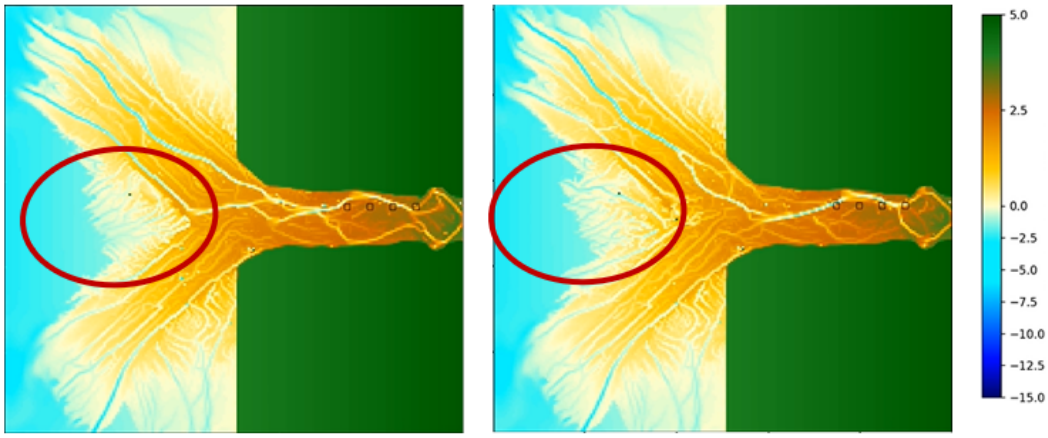

(b) 50-year dredging scenario

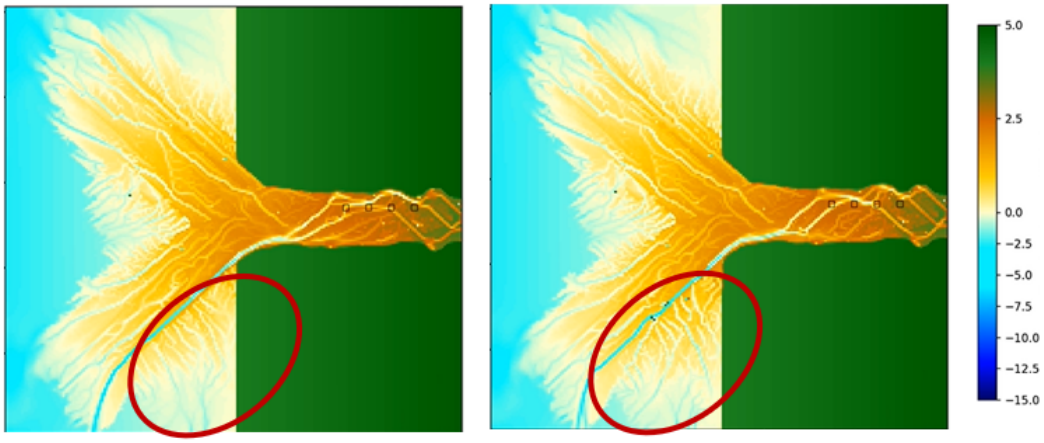

(c) 10.0x dredging intensity scenario

Figure 3.2: Comparison of morphological outcomes around the peaks illustrated in Figure 3.6, for three key dredging scenarios.

A final thing to see from visually analysing the river-delta system is the behaviour of the river. Later on this is quantified with the Braiding Index, but structural change can already be seen in the delta. In Figure 3.3 the Changing morphology of the four pit scenario and the two pit scenario,

are plotted. The first 40 years are depicted, with a time difference of 10 years per plot. Visually they are relatively similar in the first few years, though little stream alteration has taken place. Then on later time steps, the two-pit scenario has evolved to follow a single channel, from the middle of the river to the delta. The river is deeper and broader then in the four-pit simulation and seems to have eroded more of the river bank at the start of the delta. It is noteworthy that dredging already stops after the first 10 years, so the change in outcome is determined in that first step, where the rivers still behave similarly.

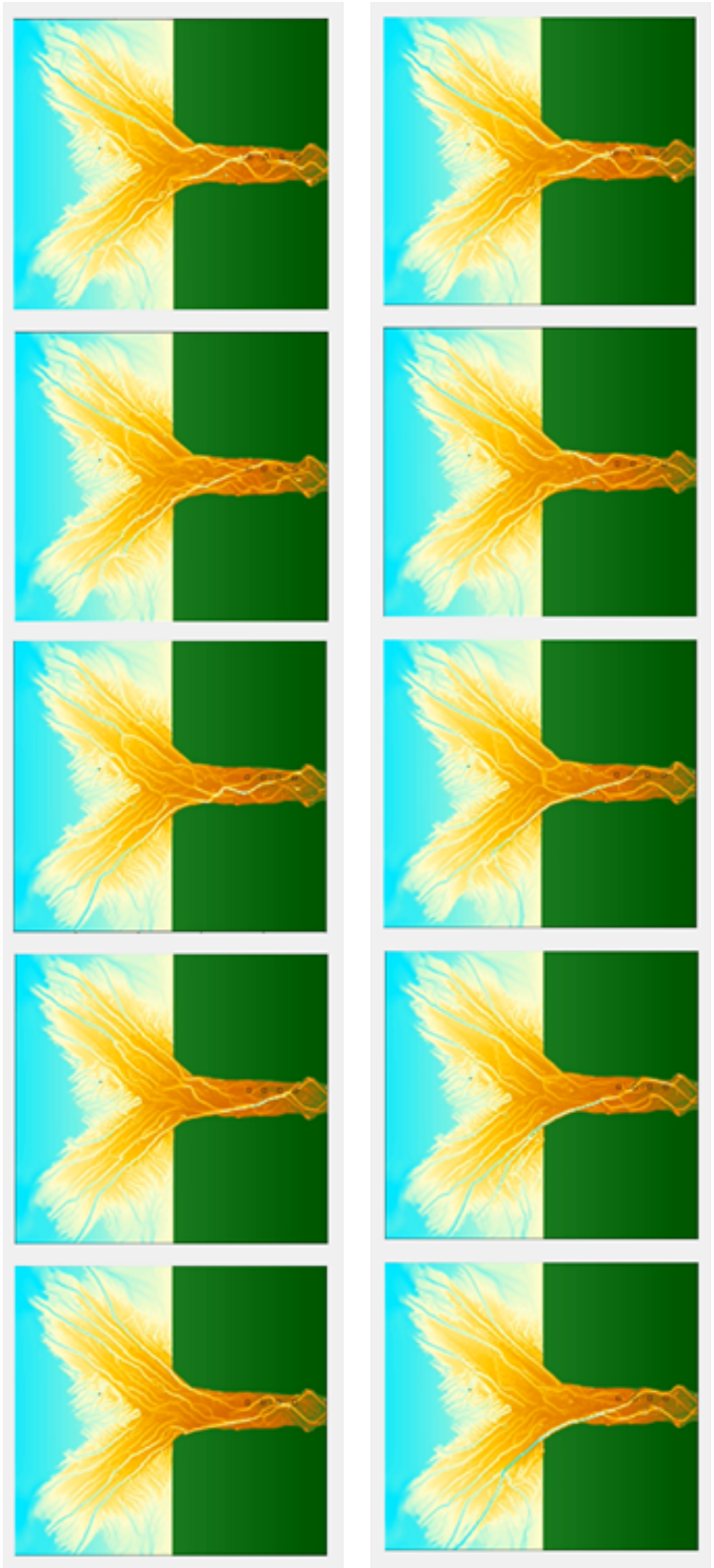

(a) four pit scenario **(b)** two pit scenario

Figure 3.3: Comparison of four locations and the two location scenarios, with t0 at the top, and a time step of 10 years between the graphs, ending at 40 years. A structural difference between the scenarios is visible as the river in the two-pit scenario has a more pronounced deeper channel.

3.2. Results per Method of Analysis

3.2.1. Delta area comparison

In Figure 3.4, the delta area is plotted across all dredging scenarios. In Figure 3.4a, most dredging scenarios follow a similar trend, with the exception of the 30-year experiment, which shows the most growth over the 100-year period. The 30-year experiment ends with the largest delta, followed by the 50-year experiment, with the remaining scenarios following closely. In Figure 3.4b, the effects of varying dredging intensities are shown. Initially, the deltas grow in a similar fashion, but after 50 years, the 5.0x simulation results in the largest delta, while the 10.0x simulation produces the smallest delta. In Figure 3.4c, the impact of varying dredging locations is displayed. All three simulations follow a steady trajectory, with the single-location scenario ending up with the smallest delta, and the two-location scenario producing the largest delta. In Figure 3.4d, delta size over time is shown for varying mining pit widths. The 200-meter-wide pit grows the fastest during the 15–30 year period, but is later caught up by the other simulations. After 100 years, the 150 meter wide pit results in the largest delta, and all scenarios produce larger deltas than the 50 meter wide control group. Finally, in Figure 3.4e, the effect of pit length is shown. Here, the delta grows similarly across all simulations, with the 100 and 150 meter long pits ending with the largest deltas, and the 200 meter long pits resulting in the smallest delta.

The overall the trend suggested by the graphs is that different sand mining strategies do not lead to consistent or predictable outcomes in long-term delta growth. For example, simulations involving the widest dredging pits (200 meters) show the fastest initial expansion, but this growth later stabilizes, resulting in a smaller delta by the end of the simulation period. In contrast, scenarios with half-intensity dredging (0.5x) initially yield the smallest deltas after 60 years, yet continue to grow and end with the second-largest delta at the 100-year mark.

These observations highlight the model's sensitivity to initial conditions. The system's behaviour appears to be governed by complex, possibly stochastic dynamics, rather than following a clear, deterministic pattern. There is no consistent relationship between the dredging scenarios and the final delta size. Furthermore, the graphs reveal no significant or deterministic difference between the dredging scenarios and the control group, where no dredging occurred.

3.2.2. Growth Rate of the Delta

The growth rate of the delta is the difference in delta area over a 10 year period. This is calculated for every 10 years and plotted in two sections. First we look at the initial period, the first 40 years, this is the period where dredging is taking place, and the direct response can be observed. And second, we take a look at the the growth rate over the whole simulation period, in order to see if there are long term effects visible.

The initial 40 years (Figure 3.6) illustrated a variety of changes caused by the scenarios. All seems to have an impact on the initial growth period. The Duration seems to behave consistent, which is to be expected, through the other simulations seem to behave quite different from each other, the 200 meters wide pit is growing the fastest of the width scenario, and for the intensity the peak is for the 5.0x scenario. The effect of the width of the pit seems to behave exponentially, and also for the length of the pit, the at the higher values result in the higher growth rates.

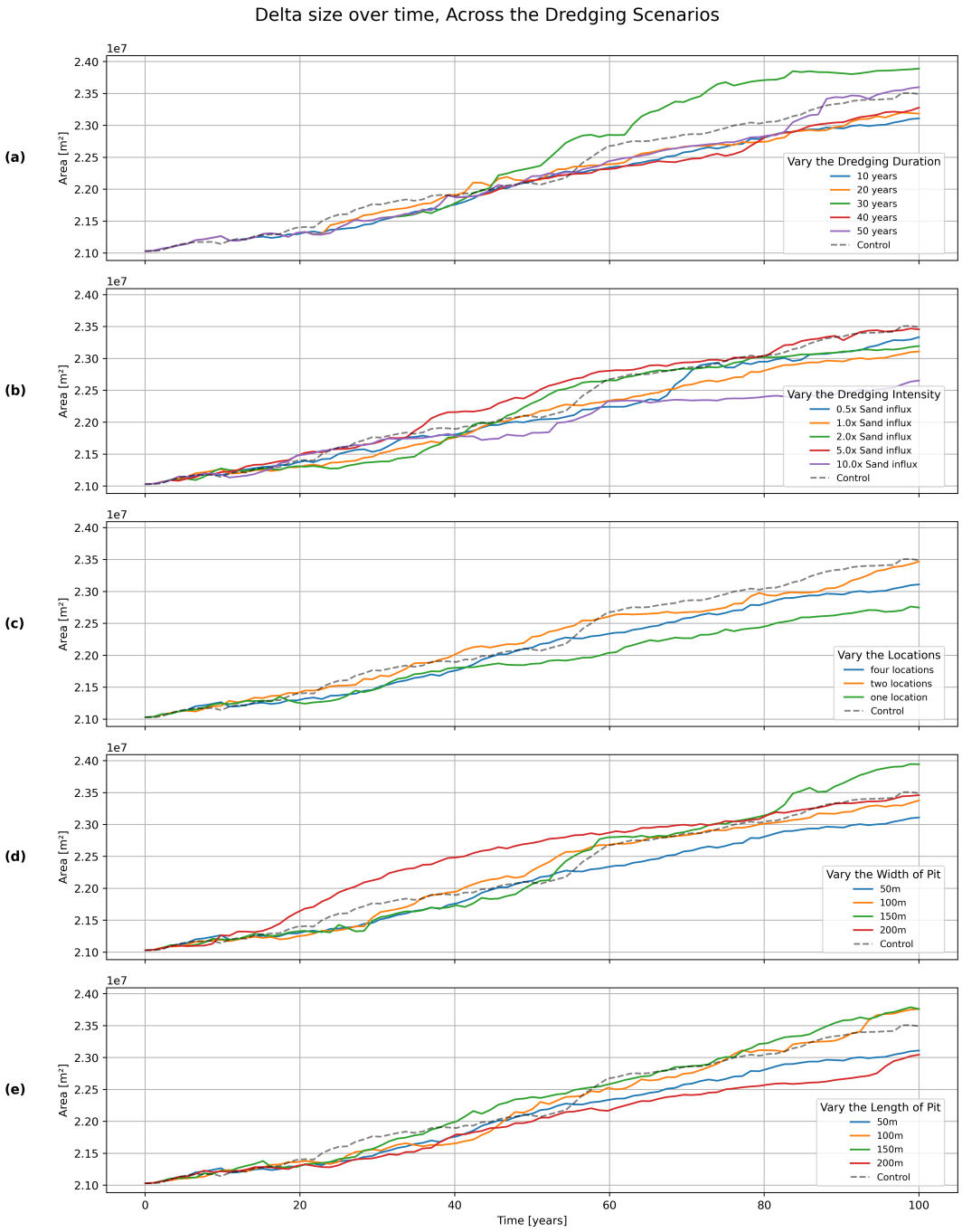

Figure 3.4: Delta Size of all the scenarios.

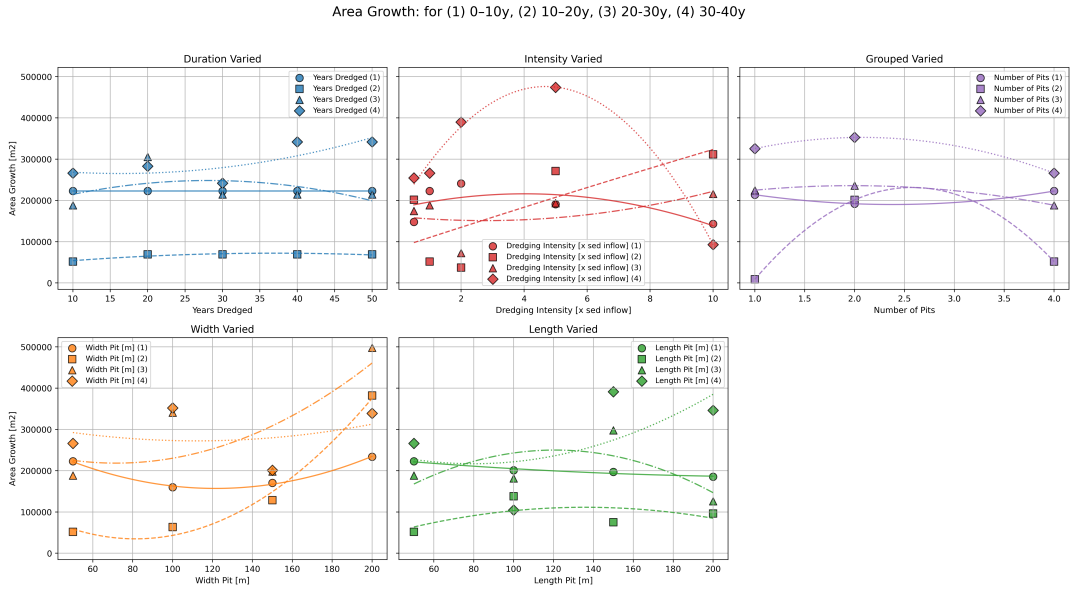

Figure 3.5: The growth rate for initial 40 years, plotted with a polynomial fit with 2 variables. Plotted for each variable.

In Figure 3.6 the growth rate is plotted over the whole simulation period. Here it is also illustrated that, all scenarios initially grow slower than the control. Then, The 30- and 50-year scenarios deviate most (3.6a) in the first scenario, with a noticeable growth spike in the 50- year scenario, also seen in the control scenario. The 1.0x and 2.0x intensity scenarios (3.6b) grow more slowly between years 10–30, while the 10.0x case grows quickly at first but ends with the smallest delta. In contrast, the 5.0x scenario results in the largest delta (3.4b), suggesting higher intensity doesn't always reduce growth. Two-location dredging (3.6c) shows the highest overall growth, with a dip between years 10–20 before rebounding. The 200-meter pits grow fastest early on but slow after year 50, while the 50–150 meter pits gradually recover (3.6d). Finally, pit length shows similar trends across scenarios, with early growth exceeding the control before crashing under it and then fluctuating around it (3.6e).

Overall, there appears to be a peak in the growth rate at year 50–60, which occurs at the control scenario and at various other scenarios. This is further looked at in the visual analysis (3.1).

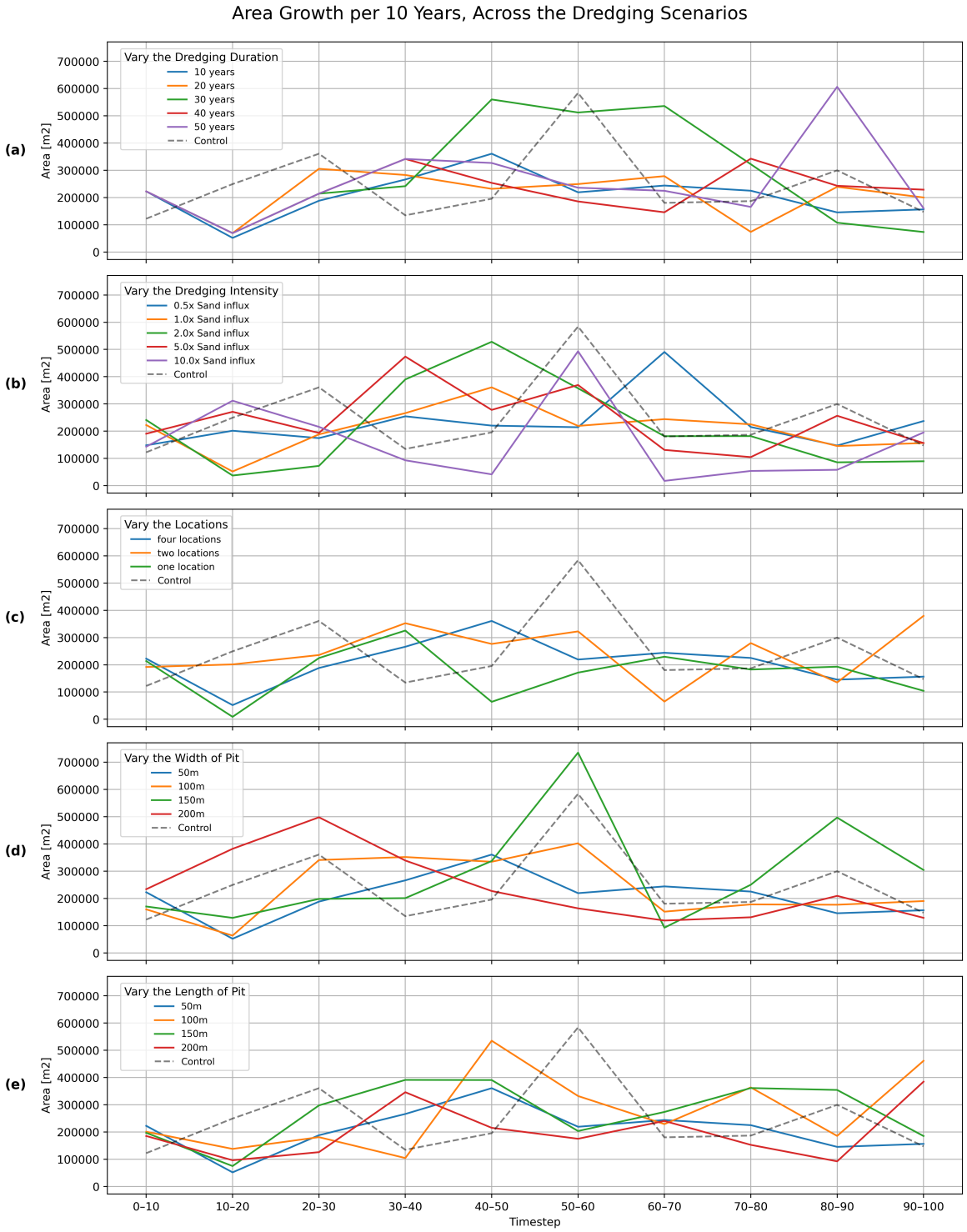

Figure 3.6: Fractional Growth rate per 10 years.

3.2.3. Braiding Index

The Braiding Index (BI), is a metric used to characterise the extent of a river network. It mostly follows a sinusoidal pattern. In Figure 3.7 the average BI over the whole simulation period is plotted and the BI distribution is plotted for time steps t50 and t100 in Figure 3.8. Here the entire river section is sliced in order to produce an comprehensive view of the structure of the river. The distribution is then tested, using a two sample Kolmogorov-Smirnov test, to see if the structure is significantly different (Table 3.1).

Looking at the Figure 3.8a, the normal fit and histogram show that after 50 years, the river is characterized similarly across scenarios. However, after 100 years, the 20-year simulation appears more channelized than the others. and the 30 an 50 year simulations are also significantly different from the control scenario.

For the intensity variation (Figure 3.8b), all scenarios show patterns similar to the control at t50 and t100. Directly after the dredging period, the 5.0x and 2.0x scenarios cover the lowest and the highest BI, with the rest of the scenarios in between (Figure 3.7b). By t50, these differences have mostly resolved, and no major divergence is observed. For the grouped scenario (3.8c), the two-location scenario changes the most, it reaches the lowest BI at t50, then continues resembling the control scenario.

For the width variation (Figure 3.7d), the 200-meter scenario deviates most from the other scenarios, showing the lowest average BI for much of the simulation. Ultimately, though, the 100-meter scenario ends with the lowest index and all of the wider pits end up significantly different from the control scenario. Regarding length variation (Figure 3.7e), the 150- and 200-meter scenarios show the lowest BI directly after dredging. This appears to be caused by pit capture, where the long pits guide the water and speed up the flow.

Overall, the Braiding Index seams to behave in a sinusoidal pattern, deviating from the control in each scenario. Though rivers that are significantly different at the 50 year mark, remain significantly different at 100 years. And some rivers that are not significantly different at 50 years are different at a 100 years. This shifting braid could be temporality as it fluctuates in a sinusoidal pattern, though this one-sided change could indicate a change in shape of the sinus.

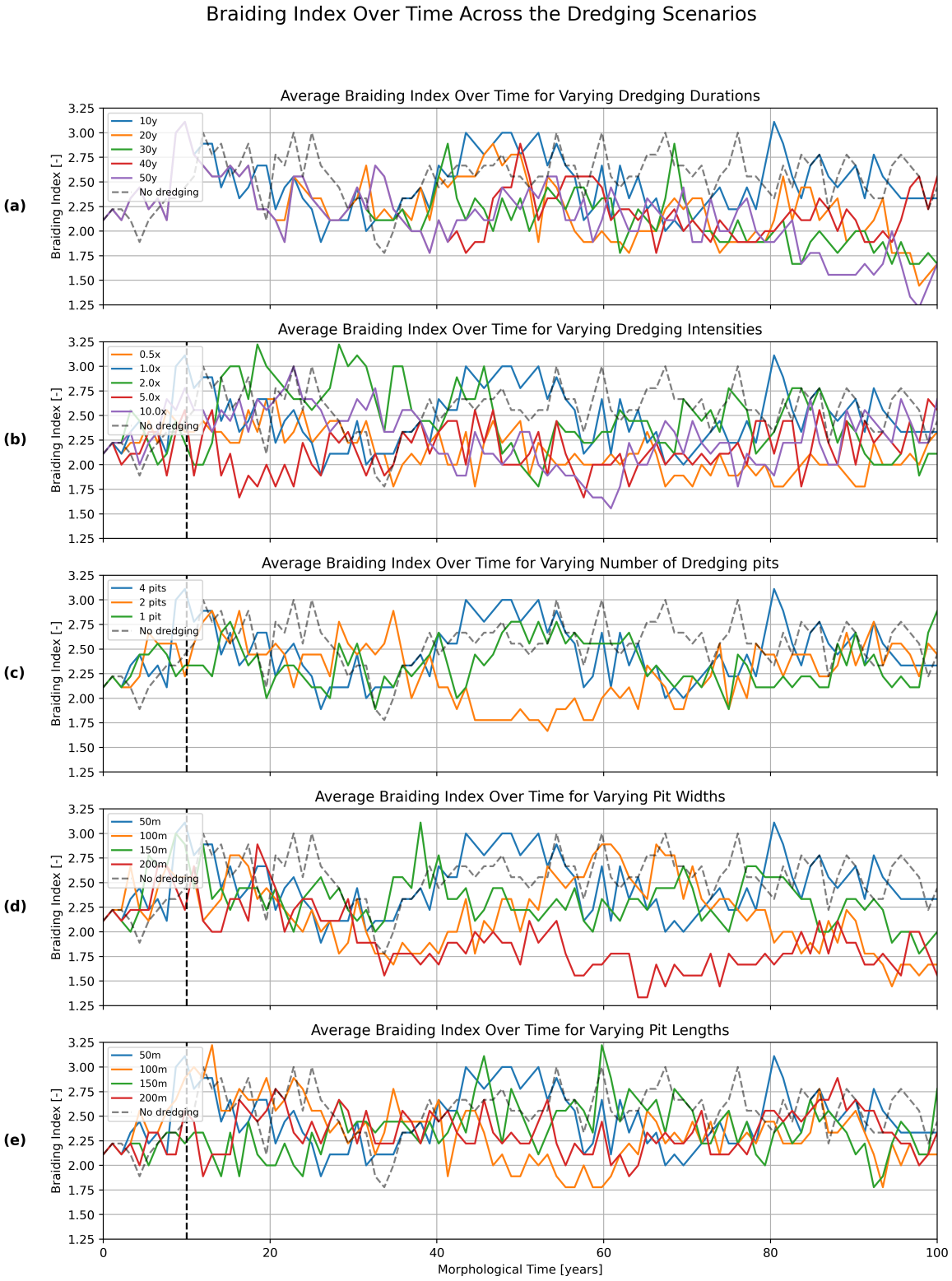

Figure 3.7: Braiding index over the river section, across each dredging scenario.

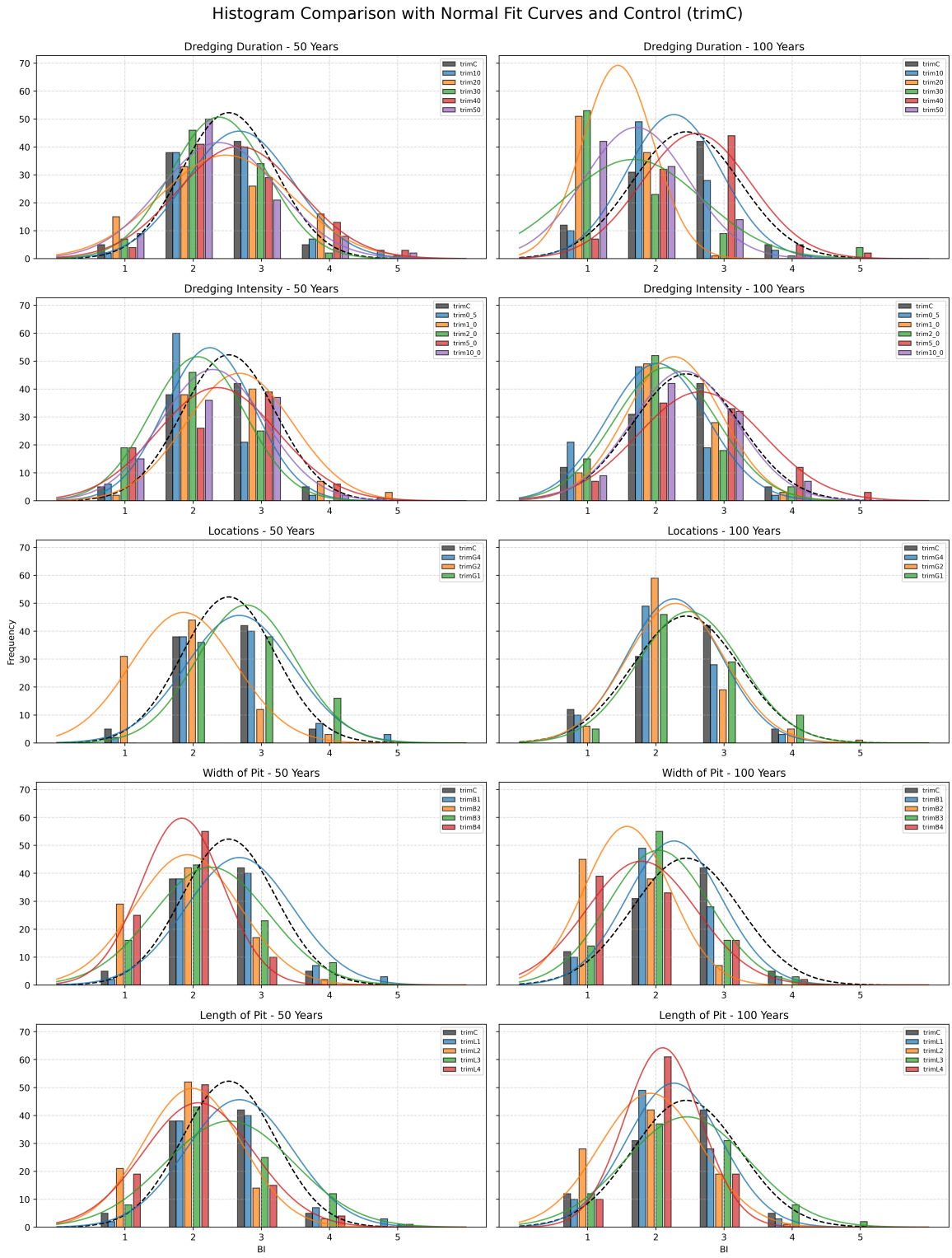

Figure 3.8: The distribution pattern of the Braiding Index at the 50- and 100-year mark.

Scenario	KS Stat (50y)	p-val (50y)	Sig? (50y)	KS Stat (100y)	p-val (100y)	Sig? (100y)
10 y dredging	0.0556	0.9992	No	0.1778	0.1164	No
20 y dredging	0.1222	0.5145	No	0.5111	0.0000	Yes
30 y dredging	0.1111	0.6378	No	0.4556	0.0000	Yes
40 y dredging	0.1222	0.5145	No	0.0556	0.9992	No
50 y dredging	0.1778	0.1164	No	0.3556	0.0000	Yes
0.5× intensity	0.2556	0.0054	Yes	0.2889	0.0010	Yes
1.5× intensity	0.0556	0.9992	No	0.1778	0.1164	No
2.0× intensity	0.2444	0.0090	Yes	0.2667	0.0032	Yes
5.0× intensity	0.1556	0.2270	No	0.1111	0.6378	No
10.0× intensity	0.1111	0.6378	No	0.0889	0.8719	No
4 locations	0.0556	0.9992	No	0.1778	0.1164	No
2 locations	0.3556	0.0000	Yes	0.2444	0.0090	Yes
1 location	0.1222	0.5145	No	0.0889	0.8719	No
50 m wide	0.0556	0.9992	No	0.1778	0.1164	No
100 m wide	0.3111	0.0003	Yes	0.4444	0.0000	Yes
150 m wide	0.1778	0.1164	No	0.3111	0.0003	Yes
200 m wide	0.4111	0.0000	Yes	0.3222	0.0002	Yes
50 m long	0.0556	0.9992	No	0.1778	0.1164	No
100 m long	0.3333	0.0001	Yes	0.3000	0.0006	Yes
150 m long	0.1000	0.7621	No	0.0667	0.9891	No
200 m long	0.3000	0.0006	Yes	0.3111	0.0003	Yes

Table 3.1: Two sample KS-test: The distribution of the Braiding Index at t50 and t100 is tested using a two-sample KS test against the control scenario. When the p-value is smaller than 0.05, the difference between distributions is significant.

3.2.4. Sediment Budget

The cumulative sediment budget is analysed across the entire river section. First, a single scenario is plotted and explained. Then, the sediment budget is compared across all scenarios and related to the control scenario.

The cross-sections where the sediment transport rates are measured are shown in Figure 3.9. The river reach is defined as the stretch between cross-section 1 and cross-section 3. To illustrate a single scenario, the cumulative sediment budget is plotted in Figure 3.10a. The "total coming in" line indicates the volume of sand entering and potentially being stored in the river reach. The "actual sediment stored" curve subtracts dredged volumes, representing the net sediment balance. In the full reach, the volume of sediment removed via dredging is about twice the volume that ends up stored. After roughly 23 years, the system appears to recover to the original sand volume within the river reach. The flattening of the curve suggests that the system reaches a form of equilibrium.

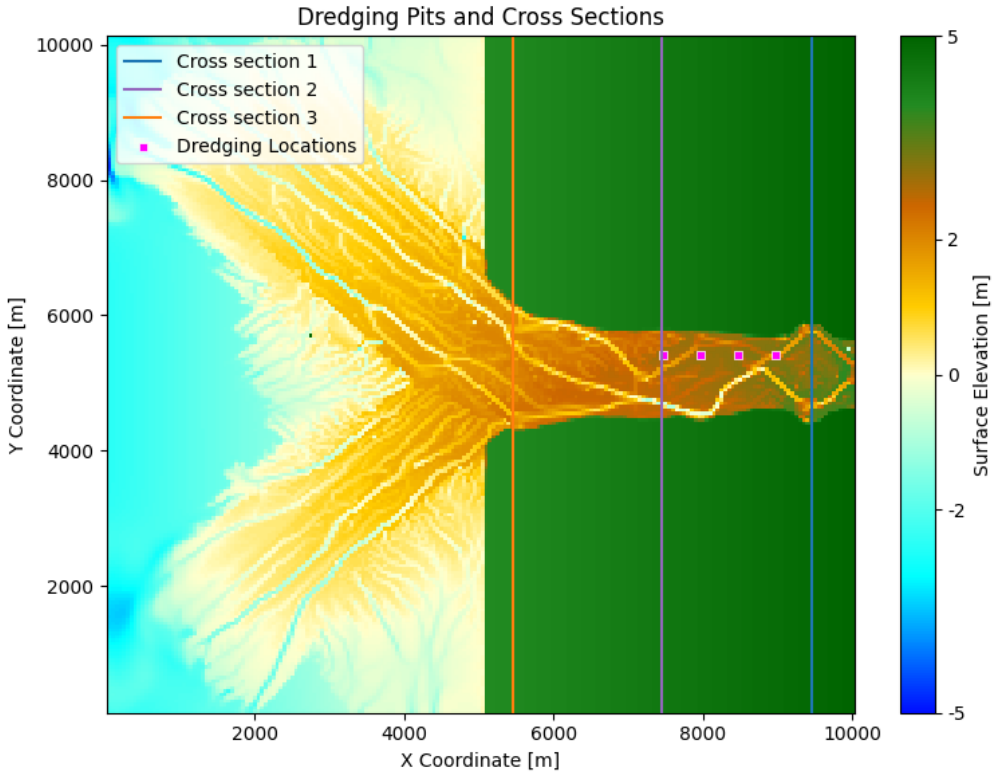

Figure 3.9: The three cross-sections: one near the upstream boundary, one just downstream of the mining pits, and one just before the delta. The dredging and river reach lie between these cross-sections.

However, the recovery is not uniform across the reach (Figure 3.10b). In section 1 (the dredging zone), sediment storage only returns to zero around year 42. In contrast, section 2 (between the dredging zone and the delta) shows a peak in deposition around year 35, which then slightly decreases. The system tends to reach a new balance, though this only occurs under certain conditions. For the remaining scenarios, the sediment balance of the entire river is analysed.

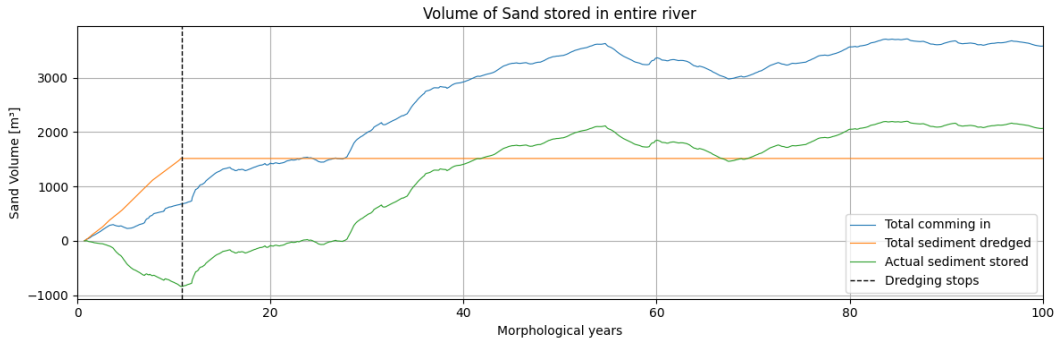

(a) Sediment balance for the full river section, alongside the dredging rate for the 10-year scenario.

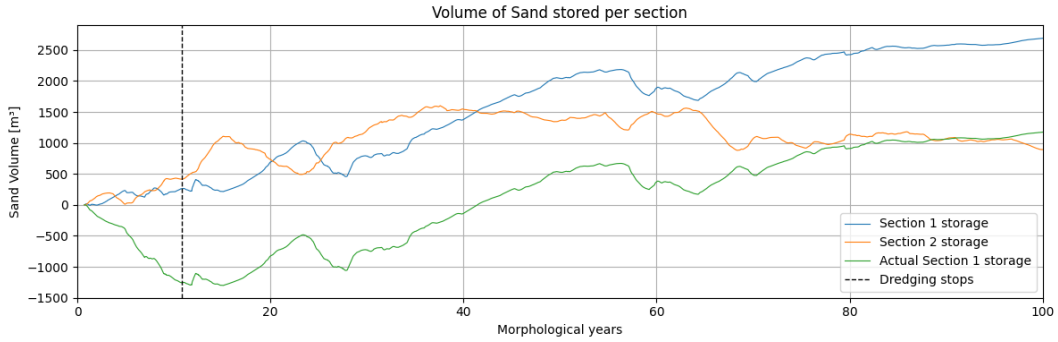

(b) Sediment balance for the two main sub-sections: section 1 (dredging area) and section 2 (between dredging and delta), for the 10-year dredging scenario.

Figure 3.10: Sediment balance under the 10-year dredging scenario. (a) Full river reach. (b) Sub-section detail focusing on the dredging area and the downstream section.

For further analyses, the dredging simulation over the whole reach it taken (Figure 3.11). Looking at the dredging duration, the 10 year scenario has the largest positive balance which is in line with the smaller delta, though a larger balance does not necessarily lead to a smaller delta as is seen for example in the width variation, where the 150-meter pits end up with the largest sediment balance and not the largest delta.

The intensity scenario (3.11b), show a clear split, where the 1.0x, 2.0x, and 5.0x scenarios end with positive sediment balances, meaning sediment is being stored in the river section. The 0.5x and 10.0x scenarios have negative sediment balances, indicating that more erosion has taken place.

The two-location scenario (G2) has the smallest sand balance (3.11c, suggesting more sediment was transported downstream. And that checks out: G2 ends up with the largest delta of all the grouped experiments (3.4c).

For the width variation scenarios (Figure 3.11d), the sediment balances align with expectations at the extremes. The 200-meter wide pits show the lowest sediment balance, indicating enhanced erosion, while the 50-meter pits have the highest. However, the 100-meter and 150-meter cases do not follow a clear pattern, suggesting that pit width alone does not consistently govern sediment dynamics across the reach.

In the length scenarios (Figure 3.11e), the 100-meter long pits behave most similarly to the control scenario in terms of sediment balance. The remaining scenarios all result in positive sediment balances after 100 years, with the 50-meter pits achieving the highest. This suggests that shorter pit lengths tend to promote more sediment storage within the river reach over time.

In general, on the long term there does not seem to be a direct relation between one of the scenaios and the outcome of the sediment budget in the short- and long-term.

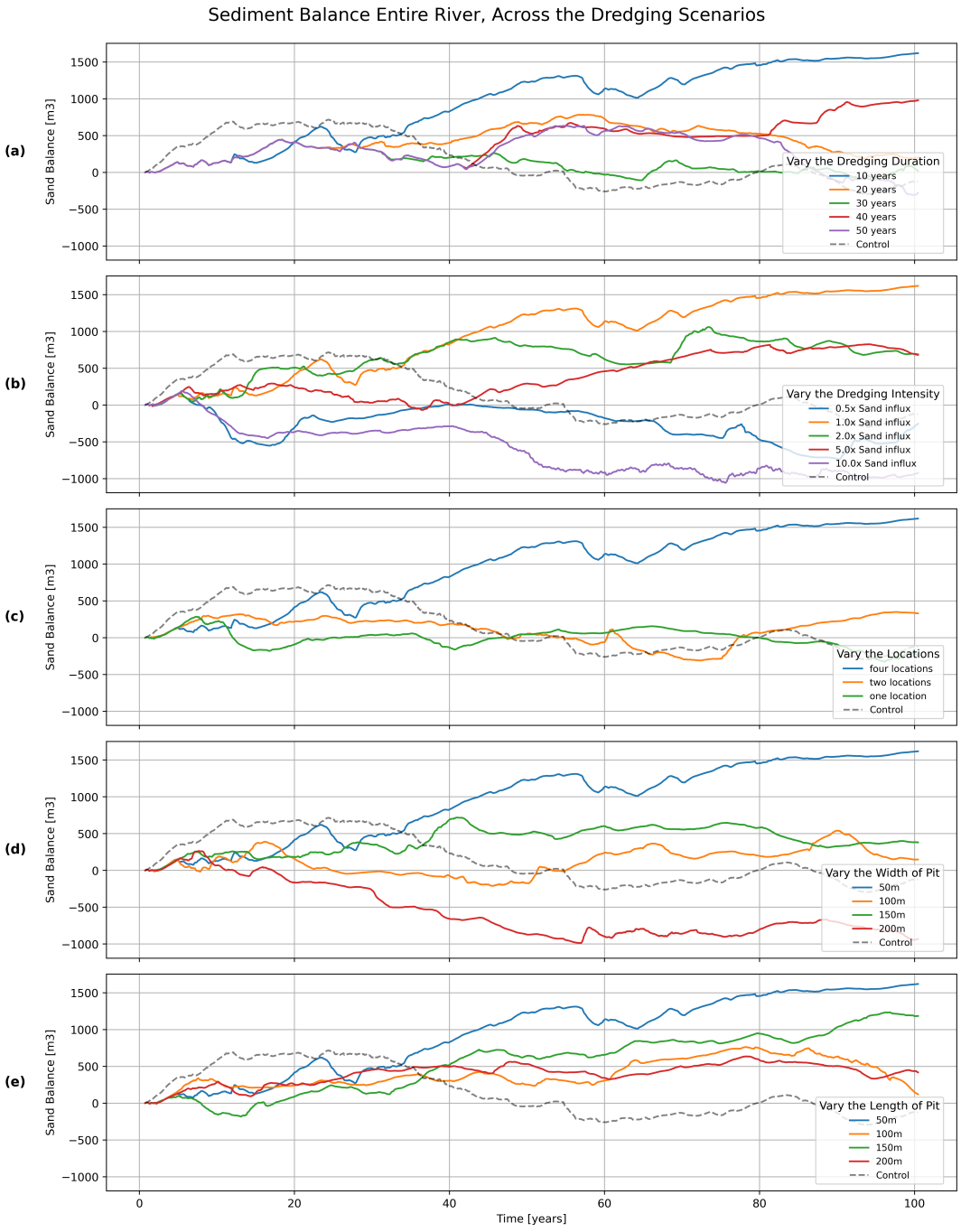

Figure 3.11: Overview of sediment balance across the full river reach.

3.2.5. Rate of Change

To quantify how the river evolves over time, we look at how much of the riverbed experiences erosion or deposition. Specifically, we calculate the total number of river cells that change by more than 0.10 meters, a practical threshold similar to the minimal required depth for calculation, to highlight morphologic change.

This gives a good idea of how dynamic the system is, and how each dredging scenario affects the rate and extent of riverbed adjustment. Erosion and deposition rates across the scenarios do not show a clear or consistent relationship with dredging parameters such as duration, intensity, or geometry. In the dredging duration (Figure 3.12a) experiment, rates fluctuate without a strong pattern, indicating that the timing of dredging does not directly dictate morpho-dynamic activity. In the intensity scenarios (3.12b), even though sediment balances differ greatly (3.11b), the erosion and deposition rates are surprisingly similar. In the 0.5x and 10.0x cases highlighting the system's internal variability. In the grouped scenarios, deposition generally exceeds erosion, especially in the G2 case, where slower initial changes are linked to greater sediment transport downstream and faster delta growth. The width scenarios (Figure 3.12d) show that the 200-meter pits have the most extreme early erosion and deposition, peaking between 15 and 20 years before declining, while the narrower pits display more moderate and gradual behaviour. Finally, in the length experiment (Figure 3.12e), all scenarios exhibit relatively stable rates over time, with only minor short-term deviations. Overall, erosion and deposition speeds appear to be governed more by complex system dynamics than by any single dredging parameter, suggesting a non-linear and sometimes unpredictable morphologic response.

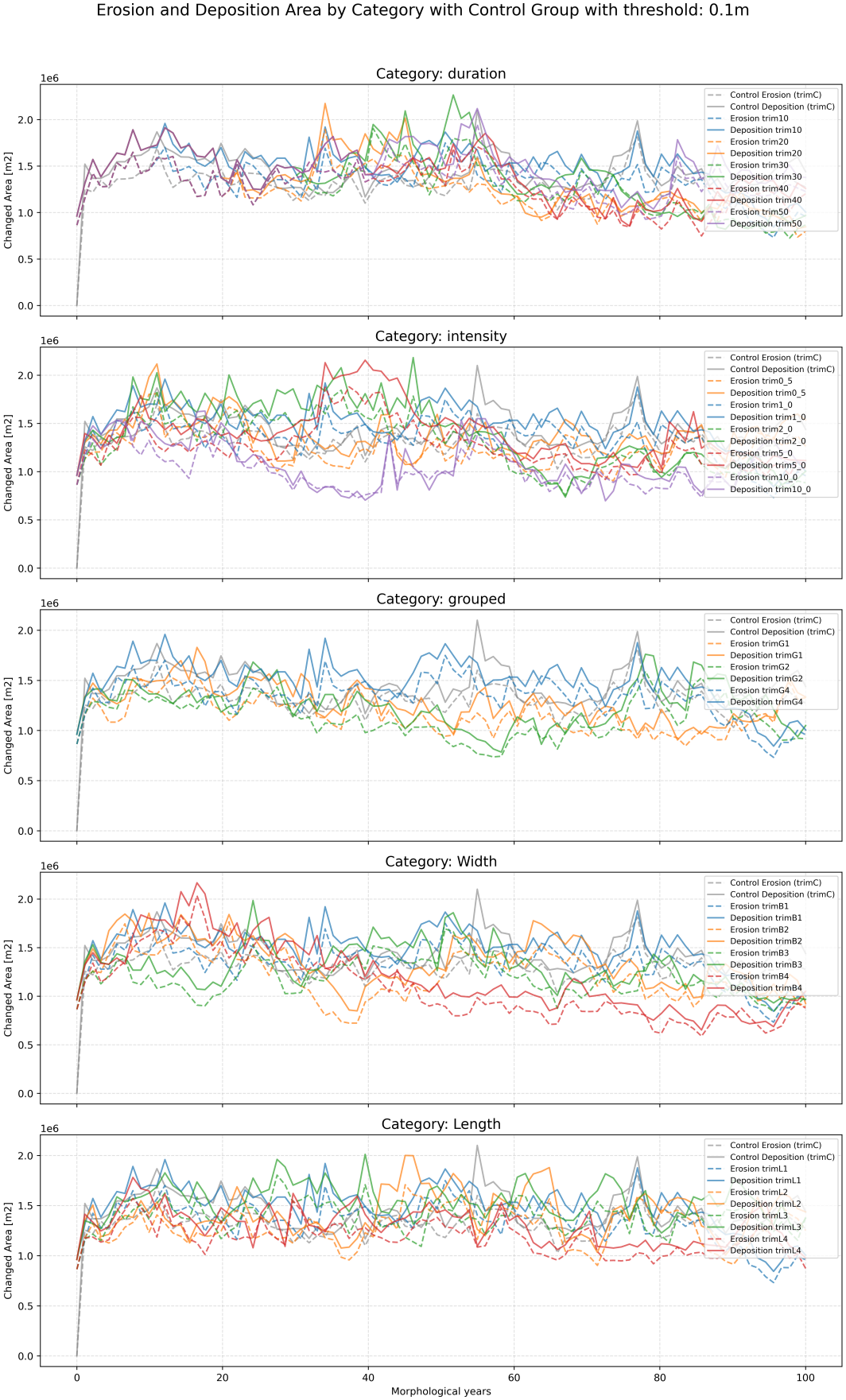

Figure 3.12: Erosion and deposition area (in number of cells) using a 0.10-meter threshold.

3.3. Results per Scenario Analyses

Before we have looked at the results per method of analyses, here there is a short summary of the findings per scenario.

In scenario 1, five dredging durations (10, 20, 30, 40, and 50 years) were tested. In the first years, all scenarios showed slower delta growth compared to the control scenario. The delta in the 30-year scenario had the most pronounced growth, followed by the delta in the 50-year scenario. This extra growth in the 30- and 50-year cases is also reflected in a sudden increase in growth rates. Regarding sediment balance, the 10-year dredging scenario stored the most sand in the river reach, with others having a lower total sediment budget, but showing similar behaviour to each other. Structurally, rivers were alike at 50 years, but at 100 years, the 20-year scenario appeared more channelized. The braiding index fluctuated sinuously over time, suggesting temporary decreases in braiding. Erosion and deposition rates showed no clear correlation with dredging duration. In short, channel complexity tends to decrease long-term, but dredging effects appear variable: the 30-year scenario had the greatest delta growth, the 20-year scenario the most structural change, and the 10-year scenario the largest sediment balance difference.

In scenario 2, five dredging intensities (0.5x, 1.0x, 2.0x, 5.0x, 10.0x sediment input) were tested. The 1.0x and 2.0x scenarios showed slower delta growth between years 10–30 compared to the control. The 10.0x scenario grew quickly initially but ended with the smallest delta long-term, while the 5.0x scenario produced the largest delta, exceeding the control. This supports the idea that higher dredging intensity doesn't necessarily reduce delta growth. Sediment balance split the scenarios aswell: 1.0x, 2.0x, and 5.0x had positive sediment storage, whereas 0.5x and 10.0x showed net erosion. However, erosion and deposition rates over time did not clearly reflect these differences. Channel structure and braiding index patterns were similar across scenarios by year 50 and 100, despite short term fluctuations especially in 2.0x and 5.0x, the 0.5x and the 2.0x show structural differences from the control scenario. Overall, no clear relationship is indicated between dredging intensity and delta development. Early variations lead to divergent long-term outcomes, suggesting nonlinear system behaviour and significant internal variability.

In scenario 3, three grouped dredging setups were tested: one (G1), two (G2), and four (G4) mining locations. Most variables followed control-like patterns, with key differences in sediment balance and delta growth. The river in scenario G4 stores the most sand compared to the rivers in G1 and G2. And for the first 50 years, the delta with two mining locations grows steadily, later caught up by the other scenarios. The braiding index shows similar behaviour between G1 and G4, while G2 consistently has the lowest BI and is the only scenario which pases the KS-test, and thus is different then the delta in the control scenario. When looking at the BI at t50 and t100, G2 changes the most; however, by the t100 mark, all scenarios resemble the control scenario again.

In scenario 4, Four pit widths were tested: 50, 100, 150, and 200 meters. The 200 m pits showed the fastest initial delta growth and the lowest sediment balance, which could indicate the most erosion. Erosion and deposition peaked around 15–20 years, then declined, becoming the slowest after 50 years. In contrast, the 50, 100, and 150 m scenarios started slower but gradually aligned with the control. Structurally, the delta in the 200 m scenario also showed the lowest braiding index for most of the simulation, though the delta in the 100 m pit scenario had the lowest BI at the end. The 100 and 200- meter scenario are significantly different from the control group and at t100, this includes the 150- meter scenario. The sediment balance ended up in a neat order, where the river in the 200 m scenario had the lowest, 50 m the highest and the 100 m and 150 m scenarios in between. Overall, wider pits lead to faster and more intense changes early on, but width alone does not reliably predict long-term sediment dynamics. Overall, the width scenario

deviate strongly from the control scenario. Though a linear pattern is not directly indicated.

In scenario 5, In the length experiment, four pit lengths were tested to evaluate their impact on delta and river behaviour. Initially, all scenarios showed a slightly faster delta growth than the control, but this was followed by a slowdown, suggesting an early disturbance and a delayed response to dredging. Over time, delta area fluctuations became more random, indicating that pit length does not produce a consistent long-term trend. Sediment balance result showed positive balances at the end for all of the scenario. steadily increasing, all differing form the control scenario. The sudden changes in budget may represent a threshold beyond which system behaviour starts to diverge. River structure, measured through the braiding index, showed minor differences shortly after dredging, especially in longer pits. At t50 and t100, both the 100- and 200- meter show significantly different structure compared to the control. Overall, pit length appears to influence short-term dynamics directly, but are the long-term outcomes not predictable just from the length of the pits.

4

Discussion

4.1. Sediment Dynamics and Hypothesised Behaviour

Referring back to the introduction, where several behaviours of the delta were hypothesised—such as increased bank erosion, pit capture, pit migration, and beach erosion—these trends are rarely evident in the results presented earlier.

While extreme cases of channelisation and channel migration have been observed, specific pit migration is not. As illustrated in Section 3.3.1, after dredging has stopped, rather then migrating upstream, they remain fixed at a constant location within the river, showing little to no movement even when subjected to flowing water. Due to the scale the result, it is unclear of pit migration is occurring. Migration is a small scale effect caused by the local erosion of the nickpoint. The scouring processes could indicate pit migration. The current (50 by 50 meters) is likely too large for the identification of small nick points. Pit capture, on the other hand, is relatively common. It typically leads to river channels migrating toward the pits, where they may persist for some time. In certain cases, this results in the formation of long, single-thread channels, which are reflected in the morphological changes and in the variations of the Braiding Index.

Further evidence of pit capture can be found in Appendix B, where actual dredging volumes are calculated. These data show that the maximum dredging rates were not always achieved, suggesting that some pits may have reached their maximum depth. Given that most of the actual dredged volumes exceed 85% of the maximum, it is likely that the pits are actively refilling. This infilling is driven by the flow of water over the section, indicating that the pit has either been captured and subsequently refilled or is functioning as a permanent in-stream feature.

It was hypothesised that due to a reduced sediment flux to the delta, the delta would either stop growing or grow at a slower rate. However, none of the deltas exhibited a decrease in area, despite literature suggesting that reduced sediment supply should result in beach and dune erosion (Shaghude et al., 2012). In this model it did not occur, and a potential feedback system could be that the sand pits generate ”hungry water,” leading to increased erosion directly downstream of the mining sites. But a restored sediment balance in the delta. Evidence for this includes the elevated erosion rates.

From the results in this study, mainly the sediment budget and the delta growth graphs, it can not be shown that an increase in dredging would lead to less sediment at the coast. It is rather dependant on other varying parameters. To get a better grip on the sediment balance at the coast, it is recommended to used a model with waves or other sediment distribution methods on the coast. When a balance is achieved between river supply and coastal erosion, and if dredging would indeed lead to less sediment to the river, its consequences could better be studied as you have a clear balance to disrupt, in comparison to a fluctuating growth trend.

Though it remains inconclusive that the dredging has a negative impact on erosion downstream. Also found when comparing the control scenario and the 10x dredging intensity (Figure 4.1. Where in the control scenario, the corner is eroded further then in the dredging scenario. The addiction of the dredging has thus modified the stream, though it is likely that the edge will erode soon, as the main river is right next to it.

Furthermore, for people living alongside sand mining sites, it is important to determine whether the mining impacts river behaviour and if there are methods to minimize these impacts. The Braiding Index and the Kolmogorov–Smirnov test indicated that after 100 years, half of the scenarios showed a significantly different braiding pattern compared to the control scenario. Most of these were also significantly affected after 50 years. While this could be attributed to the general sinuosity of the river, it is noteworthy that there is no scenario that is significantly different at the 50-year mark that is not also significantly different at the 100-year mark. While this could still be attributed to variability, it provides a starting point for further analysis of the river's structural evolution.

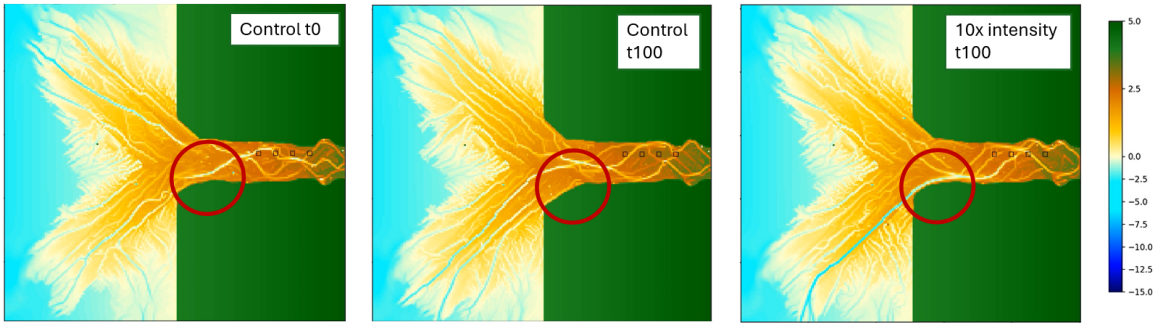

Figure 4.1: Morphology of the control scenario at t=0 and t=100, and the morphology of the 10x sediment dredging scenario, with the banks highlighted to show a change in erosion.

4.2. System Complexity and Internal Variability

While dredging clearly affects delta morphology, sediment balance, and channel structure, the long-term outcomes are highly variable and often behave in nonlinear or seemingly random ways. Across all experiments, varying dredging duration, intensity, grouping, width, and length, short-term effects are consistently observed: reduced delta growth, shifts in erosion and deposition patterns, and changes in braiding patterns. However, these short-term changes do not always translate into consistent or predictable long-term trends.

This suggests that internal system dynamics, feedback loops, and stochastic influences play a significant role in shaping outcomes. The primary feedback loop in question involves the response of water flow to subtle variations in the elevation map. Even a minor alteration in topography can significantly influence flow direction, sediment transport, and erosion patterns, potentially leading to major changes over time. Small differences early in a simulation can lead to diverging pathways, amplifying or dampening effects in unpredictable ways. The sensitivity to initial conditions, sometimes referred to as a "butterfly effect", may explain why even short or light dredging interventions occasionally produce a high variety of ourcomes.

For example, Haghnazar et al. (2020) identified optimal pit geometries based on relative stream depth and width, focusing on localized pit interactions over short time scales (minutes to hours). In contrast, this study examines system-wide effects over decades of continuous dredging. While Haghnazar found distinct relationships between pit spacing and erosion, our results suggest

that when scaled up in space and time, these geometric differences become less dominant, and system-scale responses take over.

Overall, while this study supports the idea that dredging significantly influences delta systems, it also highlights how complex, nonlinear, and path-dependent these responses can be. Rather than clear thresholds or linear relationships, outcomes depend heavily on context, initial conditions, and system feedbacks, which may mask or override expected trends.

For future studies, it is recommended to start with a distribution of control scenarios. In this study, a limiting factor is determining whether a change in the system is actually caused by the dredging pits or by the natural variability of the system. This control scenario could be implemented with slight alterations to the starting bed levels. With more, slightly varied control scenarios, it should provide a better basis to illustrate the specific effects caused by external perturbations like sand mining.

5

Conclusion

This study investigated how the downstream morphology of a river-dominated delta responds to various sand mining practices. With a focus on sediment dynamics, channel structure, and delta growth, five scenarios are tested and compared to a control scenario without dredging. Altering sediment extraction volumes, dredging durations, pit grouping, pit length, and pit width, several aspects can be concluded.

Though changing the dredging scenarios, changes the downstream morphology and hypothesised trends—such as pit migration, increased erosion, and reduced delta growth—were partially observed. A simple connection between the sand mining and the dredging simulations cannot be shown, as results suggest a far more complex and nuanced system response than initially anticipated.

The large variation are associated with avulsion-like events, where rivers found new paths, rapidly altering deposition patterns, these shifts often occurred after dredging has already stopped, emphasising the long-term influence of early disturbances. Therefore, a deterministic prediction of morphological outcomes based on a dredging scenario, remains challenging without accounting for internal variability.

To improve the robustness of future studies, it is recommended to incorporate a broader distribution of control scenarios, including slight variations in initial conditions. This approach would help differentiate between natural variability and dredging-induced changes, providing a stronger foundation for assessing the true impact of sediment extraction on river and delta evolution.

References

Arora, S., & Kumar, B. (2024). Effect of emergent vegetation on riverbank erosion with sediment mining. Scientific Reports, 14(1). https://doi.org/10.1038/s41598-024-61315-9

Arora, S., & Kumar, B. (2025). Effects of proximity of the sediment mining pit on riverbank stability. Scientific Reports, 15(1). https://doi.org/10.1038/s41598-025-95524-7

Baar, A. W., Albernaz, M. B., Van Dijk, W. M., & Kleinhans, M. G. (2019). Critical dependence of morphodynamic models of fluvial and tidal systems on empirical downslope sediment transport. Nature Communications, 10(1). https://doi.org/10.1038/s41467-019-12753-x

Barman, B., Kumar, B., & Sarma, A. K. (2018). Dynamic characterization of the migration of a mining pit in an alluvial channel. International Journal of Sediment Research, 34(2), 155–165. https://doi.org/10.1016/j.ijsrc.2018.10.009

Bendixen, M., Best, J., Hackney, C., & Iversen, L. L. (2019). Time is running out for sand. Nature, 571(7763), 29–31. https://doi.org/10.1038/d41586-019-02042-4

Bertoldi, W., Zanoni, L., & Tubino, M. (2009). Planform dynamics of braided streams. Earth Surface Processes and Landforms, 34(4), 547–557. https://doi.org/10.1002/esp.1755

Bhattacharya, R., Dolui, G., & Chatterjee, N. D. (2019). Effect of instream sand mining on hydraulic variables of bedload transport and channel planform: an alluvial stream in South Bengal basin, India. Environmental Earth Sciences, 78(10). https://doi.org/10.1007/s12665-019-8267-3

Brownlie, W. R. (1982, January). Prediction of flow depth and sediment discharge in open channels. https://doi.org/10.7907/100z-z157

Da, S., & Billon, P. L. (2022). Sand mining: Stopping the grind of unregulated supply chains. The Extractive Industries and Society, 10, 101070. https://doi.org/10.1016/j.exis.2022.101070

De Leeuw, J., Shankman, D., Wu, G., De Boer, W. F., Burnham, J., He, Q., Yesou, H., & Xiao, J. (2009). Strategic assessment of the magnitude and impacts of sand mining in Poyang Lake, China. Regional Environmental Change, 10(2), 95–102. https://doi.org/10.1007/s10113-009-0096-6

Deltares. (2025). Delft3D-FLOW user manual [Version 4.05]. Deltares. Delft, The Netherlands.

Dodds, W. K., & Whiles, M. R. (2004). Quality and Quantity of Suspended Particles in Rivers: Continent-Scale Patterns in the United States. Environmental Management, 33(3), 355–367. https://doi.org/10.1007/s00267-003-0089-z

Edmonds, D. A., Caldwell, R. L., Brondizio, E. S., & Siani, S. M. O. (2020). Coastal flooding will disproportionately impact people on river deltas. Nature Communications, 11(1). https://doi.org/10.1038/s41467-020-18531-4

Egozi, R., & Ashmore, P. (2008). Defining and measuring braiding intensity. Earth Surface Processes and Landforms, 33(14), 2121–2138. https://doi.org/10.1002/esp.1658

Engelund, F. A., & Hansen, E. (1967, January). A monograph on sediment transport in alluvial streams. http://ci.nii.ac.jp/ncid/BA68816341

Erskine, W. D. (2008). Channel incision and sand compartmentalization in an Australian sandstone basin subject to high flood variability. IAHS-AISH publication, 283–290. http://www.cabdirect.org/abstracts/20093172808.html

Filho, W. L., Hunt, J., Lingos, A., Platje, J., Vieira, L., Will, M., & Gavriletea, M. (2021). The Unsustainable Use of Sand: Reporting on a Global Problem. Sustainability, 13(6), 3356. https://doi.org/10.3390/su13063356

Hackney, C. R., Darby, S. E., Parsons, D. R., Leyland, J., Best, J. L., Aalto, R., Nicholas, A. P., & Houseago, R. C. (2020). River bank instability from unsustainable sand mining in the lower Mekong River. Nature Sustainability, 3(3), 217–225. https://doi.org/10.1038/s41893-019-0455-3

Haghnazar, H., Sangsefidi, Y., Mehraein, M., & Tavakol-Davani, H. (2020). Evaluation of infilling and replenishment of river sand mining pits. Environmental Earth Sciences, 79(14). https://doi.org/10.1007/s12665-020-09106-z

HarvardGrwthLab. (2023). The Atlas of Economic Complexity. https://atlas.hks.harvard.edu/explore/geomap?exporter=group-1&importer=&product=product-HS92-855

Hernandez, M., Scarr, S., & Daigle, K. (2021). The messy business of sand mining explained. https://www.reuters.com/graphics/GLOBAL-ENVIRONMENT/SAND/ygdpzekyavw/

Ikeda, S. (1989, January). Sediment transport and sorting at bends. https://doi.org/10.1029/wm012p0103

Jenkins, R. L., Smith, C. G., Passeri, D. L., & Ellis, A. M. (2024). Model Sensitivity Analysis for Coastal Morphodynamics: Investigating Sediment Parameters and Bed Composition in Delft3D. Journal of Marine Science and Engineering, 12(11), 2108. https://doi.org/10.3390/jmse12112108

Kim, T. T., Huy, N. D. Q., Phuoc, N. V., Phung, N. K., & Bay, N. T. (2023). Integration of a numerical model in curvilinear coordinates with sand mining component for bottom morphology simulation. IOP Conference Series: Earth and Environmental Science, 1226(1), 012025. https://doi.org/10.1088/1755-1315/1226/1/012025

Koch, F., & Flokstra, C. (1981). Bed level computations for curved alluvial channels. Delft Hydraulics Lab.

Koehnken, L., & Rintoul, M. (2018). Impacts of sand mining on ecosystem structure, process and biodiversity in rivers. World Wildlife Fund International, 159.

Koehnken, L., Rintoul, M., Goichot, M., Tickner, D., Loftus, A.-C., & Acreman, M. (2020). Impacts of riverine sand mining on freshwater ecosystems: A review of the scientific evidence and guidance for future research. River Research and Applications, 36(3), 362–370.

Kondolf, G. M. (1997). PROFILE: Hungry Water: Effects of Dams and Gravel Mining on River Channels. Environmental Management, 21(4), 533–551. https://doi.org/10.1007/s002679900048

Langendoen, E. J. (2001). Process-based simulation of riverbank erosion [Doctoral dissertation, Technical University of Delft] [Chapter on model comparisons between Delft3D and Mike21C]. https://apps.dtic.mil/sti/pdfs/ADA387220.pdf

Lawal, P. (2011). Effects of Sand/Gravel Mining in Minna Emirate Area of Nigeria on Stakeholders. Journal of Sustainable Development, 4(1). https://doi.org/10.5539/jsd.v4n1p193

Maaß, A.-L., & Schüttrumpf, H. (2018). Long-term effects of mining-induced subsidence on the trapping efficiency of floodplains. Anthropocene, 24, 1–13. https://doi.org/10.1016/j.ancene.2018.10.001

Mosselman, E. (2004). Morphological modeling of rivers with erodible banks [Discusses validation of Delft3D with field data]. Hydroinformatics 2004, 1583–1590. https://repository.tudelft.nl/islandora/object/uuid:6a0d9a5a-faec-4b4b-b1dc-00d61c4a0837

Mouterde, P., & Depardon, M. (2023). India's 'sand mafias have power, money and weapons'. https://www.lemonde.fr/en/environment/article/2022/09/12/in-india-sand-mafias-have-power-money-and-weapons_5996639_114.html

Nguyen, B. Q., Kantoush, S. A., & Sumi, T. (2024). Quantifying the consequences of unsustainable sand mining and cascade dams on aspects in a tropical river basin. Scientific Reports, 14(1). https://doi.org/10.1038/s41598-024-51405-z

Padmalal, D., & Maya, K. (2014, January). Sand mining. https://doi.org/10.1007/978-94-017-9144-1

Padmalal, D., Maya, K., Sreebha, S., & Sreeja, R. (2007). Environmental effects of river sand mining: a case from the river catchments of Vembanad lake, Southwest coast of India. Environmental Geology, 54(4), 879–889. https://doi.org/10.1007/s00254-007-0870-z

Prins, C. (2025). Msc-thesis [GitHub repository]. https://github.com/Camu-git/MSc-thesis

Rahdarian, A., & Winter, C. (2025). Process-based numerical modelling up and down beach morphological states. Geo-Marine Letters, 45(2). https://doi.org/10.1007/s00367-025-00802-y

Rentier, E., & Cammeraat, L. (2022). The environmental impacts of river sand mining. The Science of The Total Environment, 838, 155877. https://doi.org/10.1016/j.scitotenv.2022.155877

Roelvink, D., Reniers, A., van Dongeren, A., van Thiel de Vries, J., McCall, R., & Lescinski, J. (2006). Modelling storm impacts on beaches, dunes and barrier islands. Coastal Engineering, 53(10), 749–770. https://doi.org/10.1016/j.coastaleng.2006.08.006

Schandl, H., Fischer Kowalski, M., West, J., Giljum, S., Dittrich, M., Eisenmenger, N., Geschke, A., Lieber, M., Wieland, H., Schaffartzik, A., Krausmann, F., Gierlinger, S., Hosking, K., Lenzen, M., Tanikawa, H., Miatto, A., & Fishman, T. (2017). Global Material Flows and Resource Productivity: Forty Years of Evidence. Journal of Industrial Ecology, 22(4), 827–838. https://doi.org/10.1111/jiec.12626

Schuurman, F., Marra, W. A., & Kleinhans, M. G. (2013). Physics-based modeling of large braided sand-bed rivers: Bar pattern formation, dynamics, and sensitivity. Journal of Geophysical Research Earth Surface, 118(4), 2509–2527. https://doi.org/10.1002/2013jf002896

Shaghude, Y. W., Mburu, J., Uku, J., Arthurton, R. A., Nyandwi, N., Onganda, H., Magori, C., & Sanga, I. (2012). Beach sand supply and transport at Kunduchi, Tanzania, and Bamburi, Kenya. Western Indian Ocean Journal of Marine Science, 11(2), 135–154.

Shaw, J. B., Wolinsky, M. A., Paola, C., & Voller, V. R. (2008). An image-based method for shoreline mapping on complex coasts. Geophysical Research Letters, 35(12). https://doi.org/10.1029/2008gl033963

Slingerland, R., & Smith, N. D. (2004). RIVER AVULSIONS AND THEIR DEPOSITS. Annual Review of Earth and Planetary Sciences, 32(1), 257–285. https://doi.org/10.1146/annurev.earth.32.101802.120201

Stanley, D. J. (1996). Nile delta: extreme case of sediment entrapment on a delta plain and consequent coastal land loss. Marine Geology, 129(3-4), 189–195. https://doi.org/10.1016/0025-3227(96)83344-5

Thi Kim, T., Huong, N. T. M., Huy, N. D. Q., Tai, P. A., Hong, S., Quan, T. M., Bay, N. T., Jeong, W.-K., & Phung, N. K. (2020). Assessment of the impact of sand mining on bottom morphology in the mekong river in an giang province, vietnam, using a hydro-morphological model with gpu computing. Water, 12(10). https://doi.org/10.3390/w12102912

Thorne, C. R., & Tovey, N. K. (1981). Stability of composite river banks. Earth Surface Processes and Landforms, 6(5), 469–484. https://doi.org/10.1002/esp.3290060507

van der Wegen, M., & Roelvink, J. A. (2008). Long-term morphodynamic evolution of a tidal embayment using a two-dimensional process-based model. Journal of Geophysical Research: Oceans, 113(C3). https://doi.org/10.1029/2006JC003983

Wang, Z.-F., Ding, J.-Y., & Yang, G.-S. (2012). Risk analysis of slope instability of levees under river sand mining conditions. DOAJ (DOAJ: Directory of Open Access Journals). https://doi.org/10.3882/j.issn.1674-2370.2012.03.009

WWF. (2020, February). Sand mining in the heart of the Amazon of Europe. https://www.wwf.mg/?362410/Sand-mining-in-the-heart-of-the-Amazon-of-Europe

A

Mahakam Delta

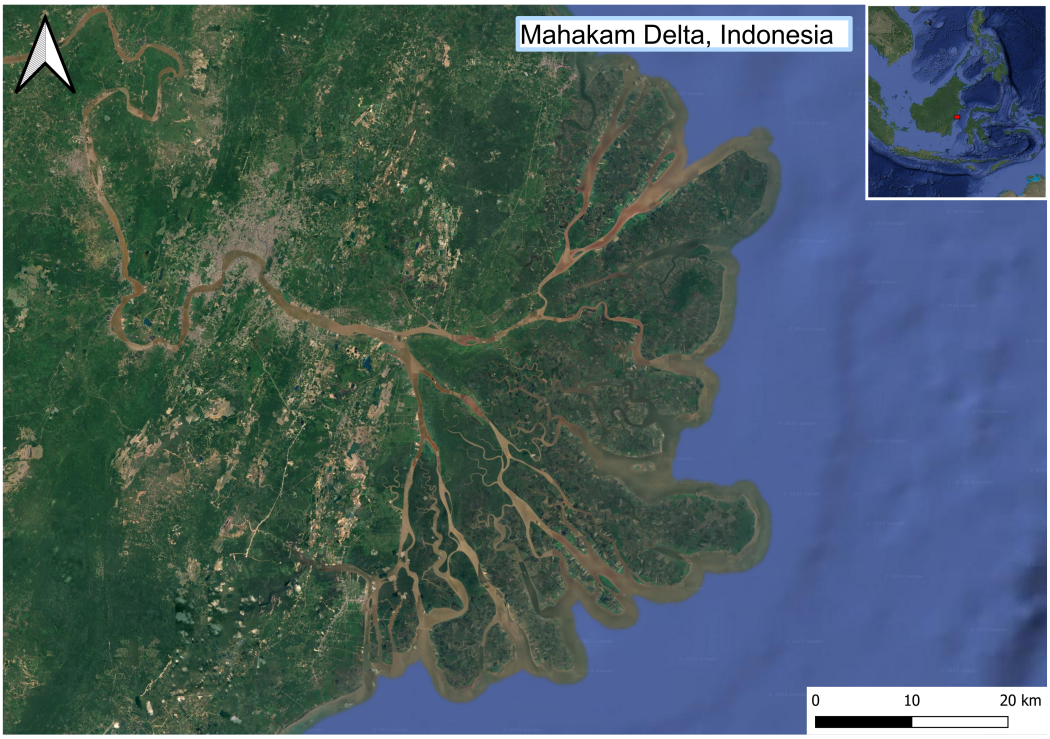

Figure A.1: The Mahakam Delta on which the Delta in this thesis is loosely based (Google Earth, 2025).

B

Actual dredging Volumes

Simulation key	Planned volume (m³)	Actual sediment volume (m³)	Fraction (%)
trih10	1760	1515.84	86.1
trih20	3520	2638.24	75.0
trih30	5280	3760.71	71.2
trih40	7040	4937.48	70.1
trih50	8800	6227.36	70.8
trih0_5	880	706.62	80.3
trih1_0	1760	1515.84	86.1
trih2_0	3520	3257.59	92.5
trih5_0	8800	7314.79	83.1
trih10_0	17600	16536.67	94.0
trihG4	1760	1515.84	86.1
trihG2	1760	1750.84	99.5
trihG1	1760	1760.00	100.0
trihB1	1760	1515.84	86.1
trihB2	1760	1609.01	91.4
trihB3	1760	1708.59	97.1
trihB4	1760	1760.00	100.0
trihL1	1760	1515.84	86.1
trihL2	1760	1741.06	98.9
trihL3	1760	1758.18	99.9
trihL4	1760	1711.61	97.3

Table B.1: Comparison of planned vs. actual dredging volumes for all simulation scenarios

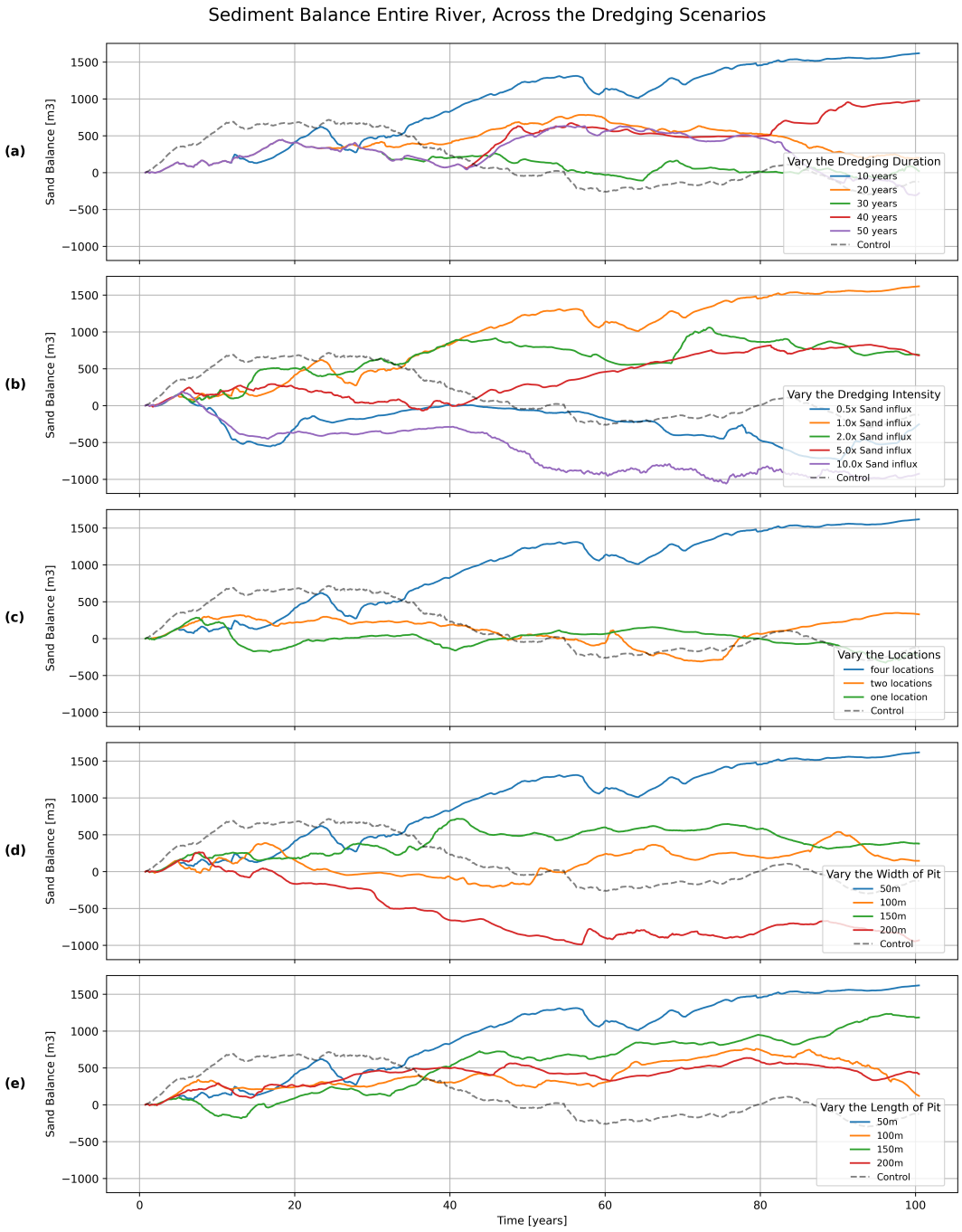

Figure B.1: Sediment balance of the whole river

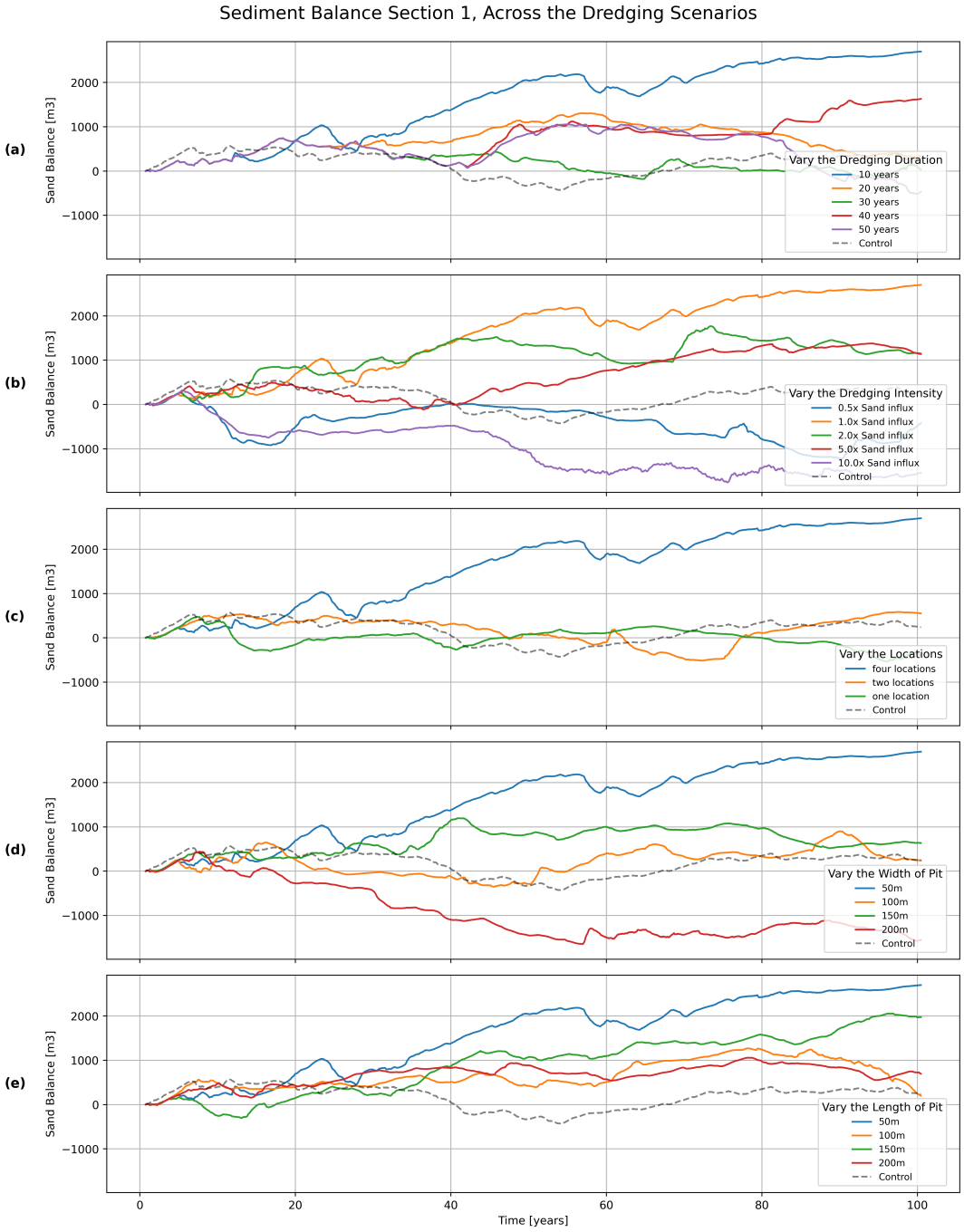

Figure B.2: Sediment balance of section 1

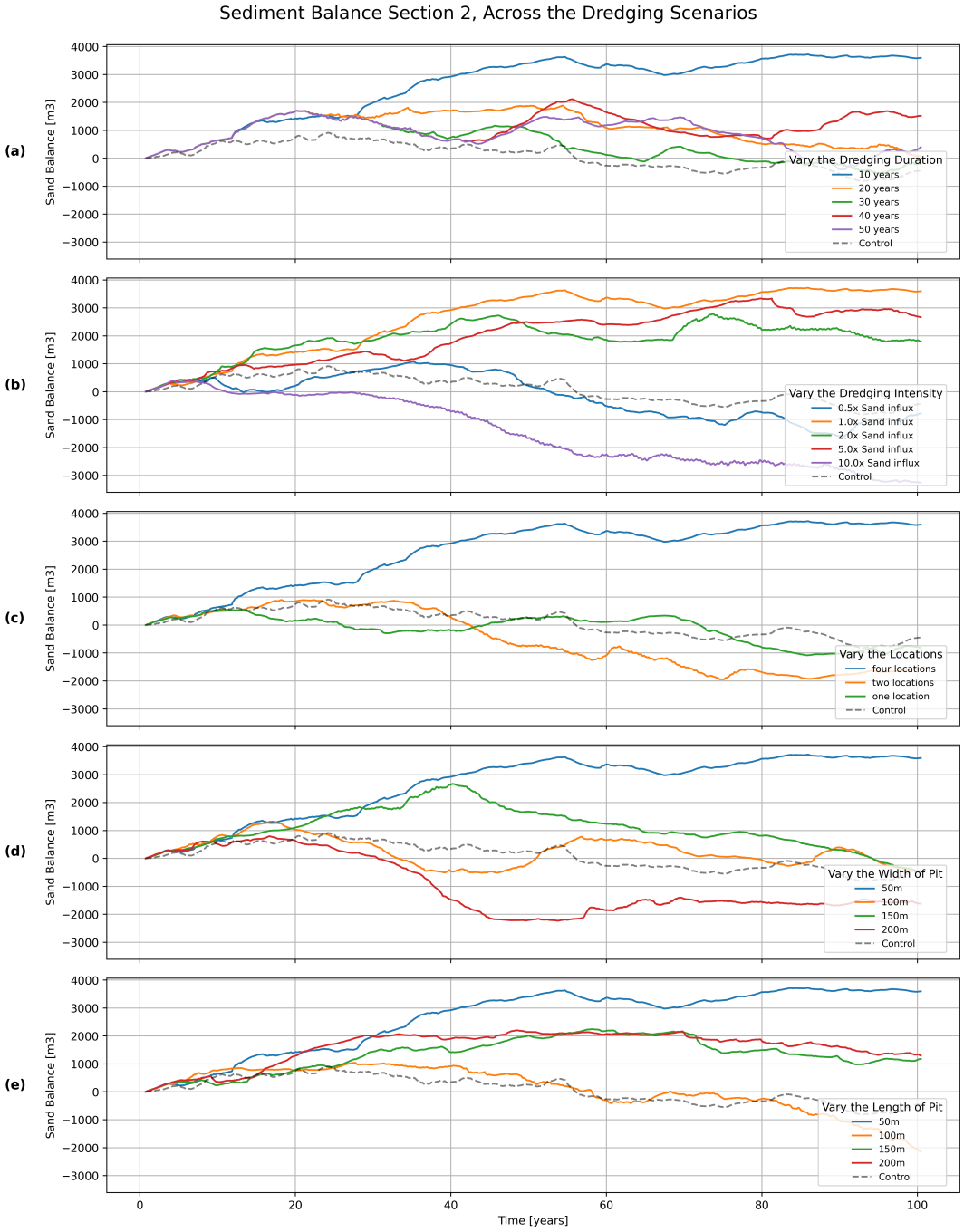

Figure B.3: Sediment balance of section 2

C

Experimental Setup Trials

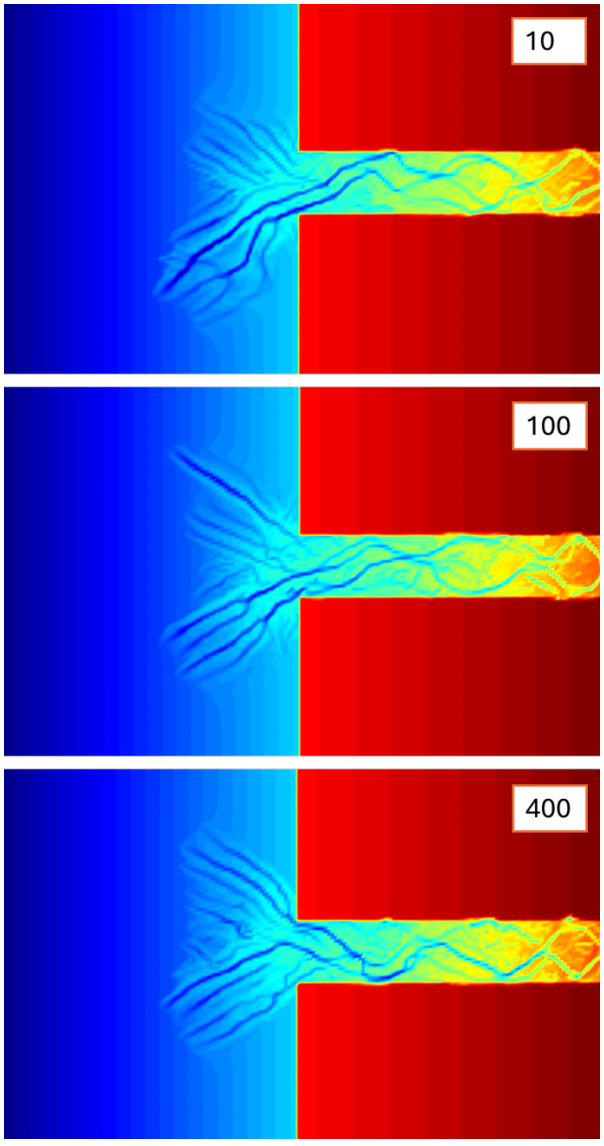

Figure C.1: Comparison of different morphological acceleration factors (MorFac = 10, 100, 400) over a 7-year simulation period to compare the effect of the MorFac. All simulations ending up with a similar morhology.

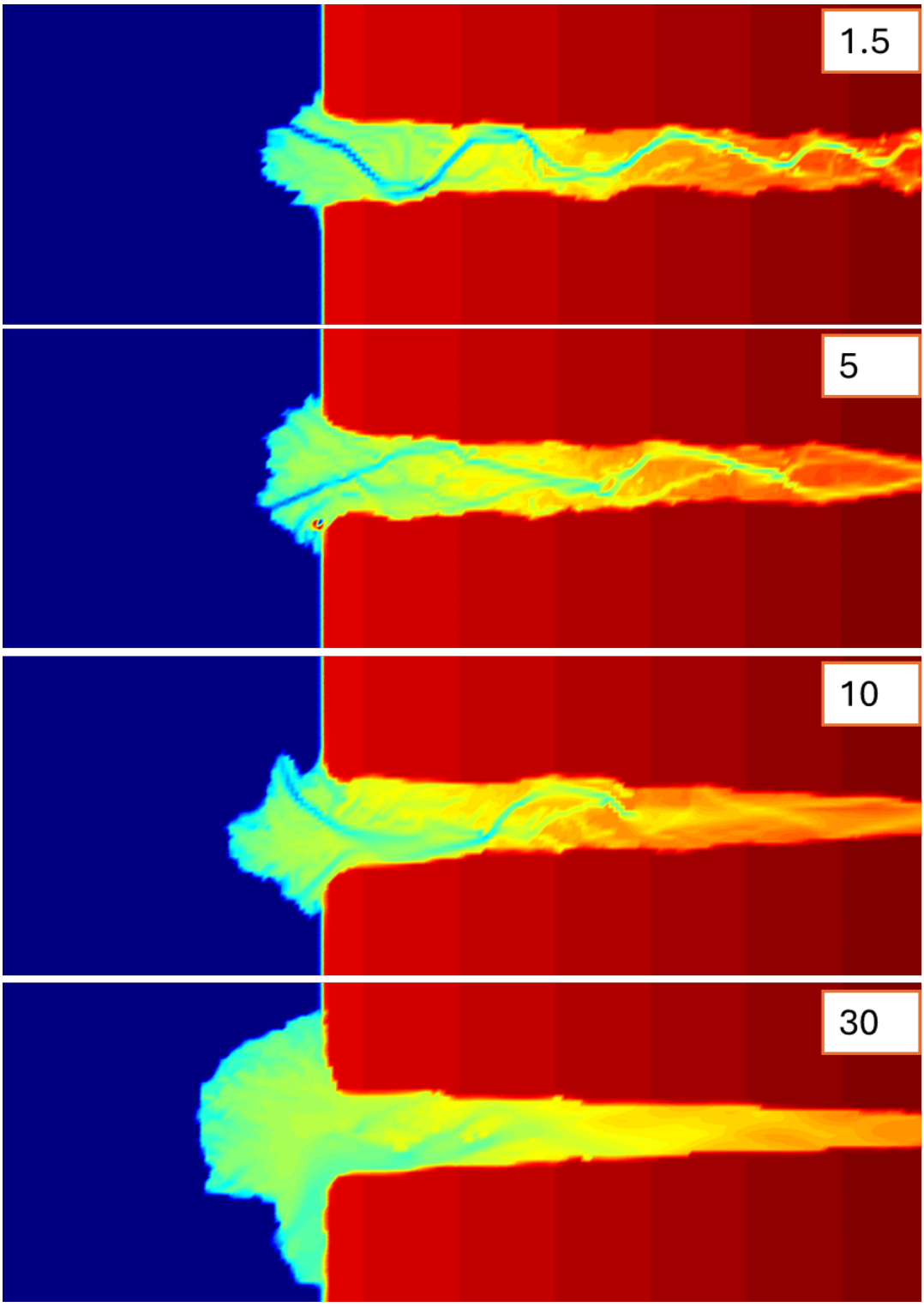

Figure C.2: Sensitivity analysis of the α_{Bn} parameter using a morphological acceleration factor (MorFac) of 100 over a 1-month hydrological simulation period. Four different values of α_{sh} were tested, where increasing value of the α_{Bn} leads to softening of the river, with almost none defined.

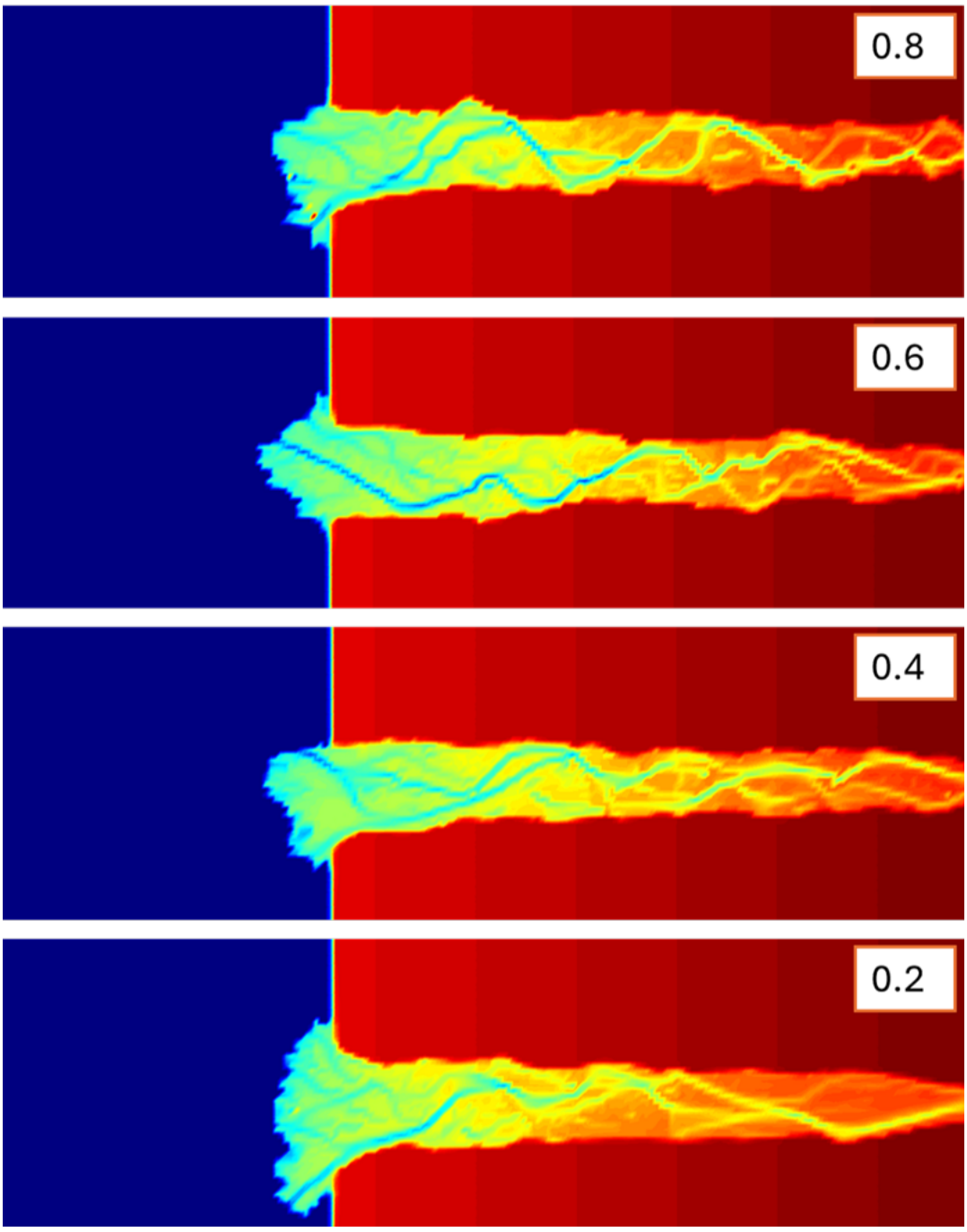

Figure C.3: Effect of varying the A_{sh} parameter over a 1-month simulation period using a MorFac of 100. Decreasing from 0.8, a lower value leads to a softer definition of the river. The most pronounced river is 0.8.

D

Delta delineation

For the full code and more notebooks behind this thesis, visit: https://github.com/Camu-git/MSc-thesis/.

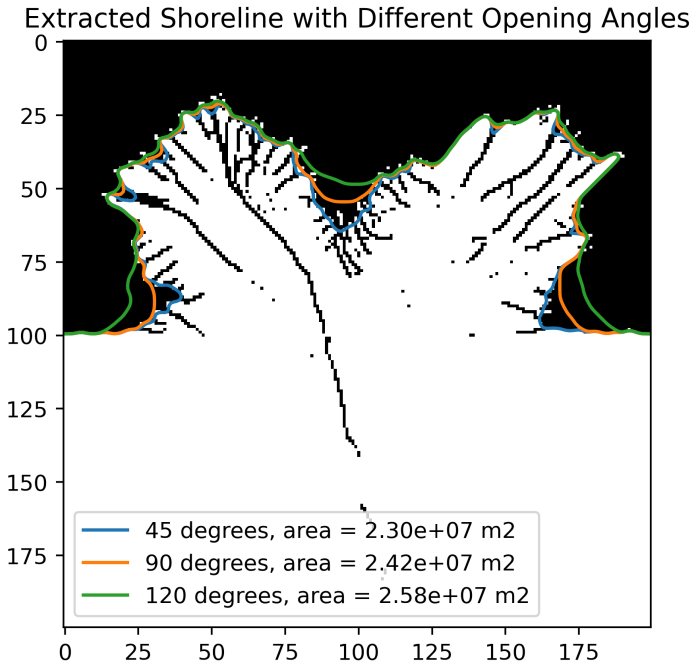

Figure D.1: Calibrating the opening angle for delineating the delta.As the 90 and 120 capture a lot of water,the 45 is chosen, It wraps closest around the Delta.

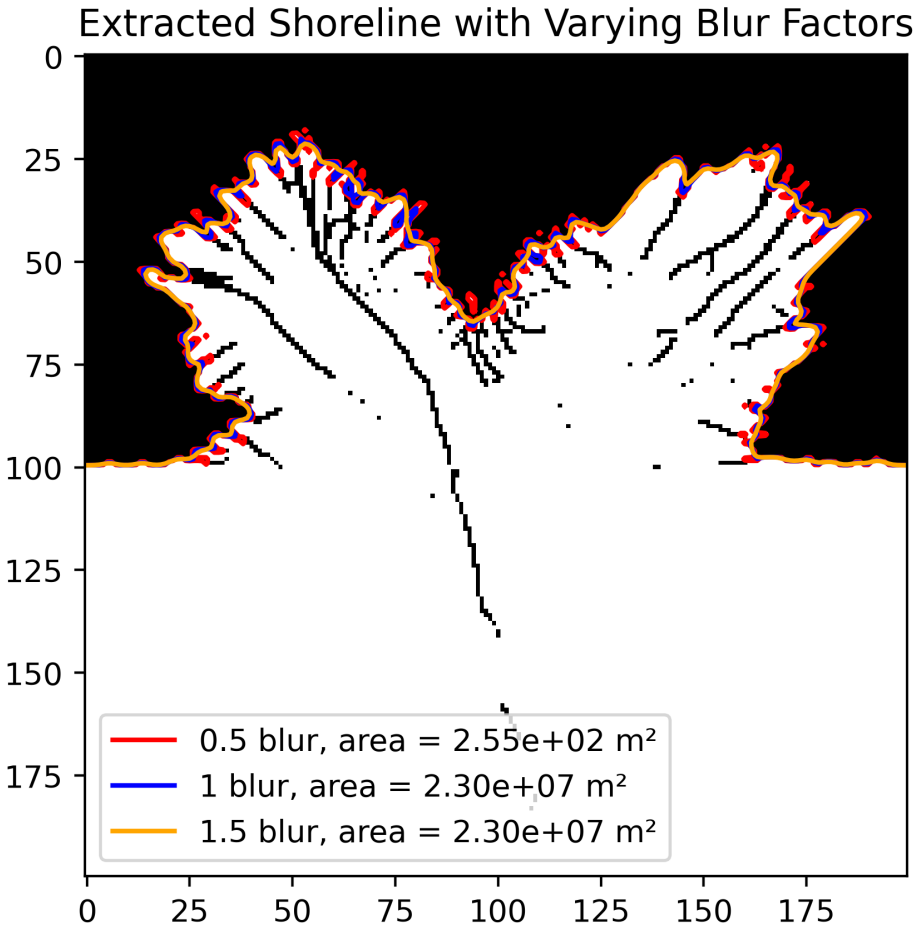

Figure D.2: Calibrating the blur factor of the delta edge. The smoother edge is chosen as it shows the edge neatly without capturing too much detail.